Netherlands Journal of Geosciences — Geologie en Mijnbouw |95 – 4 | 467–489 | 2016 doi:10.1017/njg.2016.9

Provenance signals in metaturbidites of the Paleoproterozoic greenstone belt of the Guiana Shield in Suriname

R. Naipal[1,*] & S.B. Kroonenberg[2]

[1] Department of Geology and Mining, Anton de Kom University of Suriname, Leysweg 86, Paramaribo, Suriname
[2] Department of Geoscience and Engineering, Delft University of Technology, Stevinweg 1, 2628 CN Delft, the Netherlands
[*] Corresponding author. Email: renoesha.n@gmail.com

Manuscript received: 31 May 2015, accepted: 13 March 2016

Abstract

The sedimentological, metamorphic, petrographic and geochemical characteristics of the Armina Formation, part of the Paleoproterozoic Greenstone Belt of Suriname in South America, are described, based on field, geochemical and petrographic evidence obtained through fieldwork along the Marowijne River and study of diamond drill cores from Rosebel Gold Mine (RGM). The metagreywackes show characteristic features of deposition by turbidity currents: coarse-grained, poorly sorted graded greywackes, covered by fine-grained, parallel-laminated phyllitic beds, often with convolute structures and climbing ripples. Their immature character and composition suggest deposition in an arc-trench environment. In the Marowijne River three different facies of metagreywackes are distinguished: (1) the greyish Bonnidoro Falls facies, characterised by common red millimetre-sized pseudomorphs after siderite in the finer beds, (2) the green Paroe Tabiki metagreywacke facies, with decimetre-sized calcsilicate nodules, both metamorphosed in the lower greenschist facies with chlorite as the main mafic mineral, and (3) the grey Armina Falls metagreywacke facies, geochemically similar to the Bonnidoro type but of higher metamorphic grade with biotite as the main mafic mineral. The metagreywackes from the Marowijne River show a predominance of quartz, plagioclase and lithic (tonalitic) clasts, suggesting exhumation of tonalite–trondhjemite–granodiorite plutons before deposition of the turbidites. There is a slight increase in maturity from (1) to (3), suggesting increasing weathering in the source areas. The metagreywackes of the RGM (JZone) have a predominantly metavolcanic origin, suggesting that they have a different provenance area than the Marowijne metagreywackes. Geochemically the spread in composition within each facies is larger than between the facies because of the wide range in grain sizes in each turbidite sequence. A large part of the rocks from the RGM, classified by previous authors as arenites, are geochemically and petrographically metagreywackes. Only a few RGM samples are real arenites, and plot as a separate cluster in geochemical factor score plots because of their low Fe and Na contents.

Keywords: Greenstone belt, Guiana Shield, Metagreywacke, point counting, Trans-Amazonian Orogeny, turbidites

Introduction

Turbidites are common components of Paleoproterozoic greenstone belts; they represent submarine mass flows along volcanic arcs and active and passive continental margins. We present field, petrographic and geochemical data demonstrating that different provenance areas can be distinguished in metaturbidites in the Paleoproterozoic greenstone belt of the Guiana Shield in Suriname, both laterally along the active margin and vertically in the stacked turbidite deposits. This may contribute to a better understanding of the paleogeography and sequence of events during the Amazonia–West Africa collision 2.2–2.1 Ga.

Geological setting

The Paleoproterozoic greenstone belt of the Guiana Shield stretches over more than 1500 km along the northern coast of South America, from northern Venezuela, through the Guianas to the Amapá State in northern Brazil (Fig. 1; Gibbs & Barron, 1993; Delor et al., 2003a; Kroonenberg & De Roever, 2010; Daoust et al., 2011; Kroonenberg et al., 2016). Like many other Archean and Paleoproterozoic greenstone belts, the Suriname part of the Guiana Shield greenstone belt, also called Marowijne Greenstone Belt (Kroonenberg et al., 2016), consists of a lower, metavolcanic series (Paramaka Formation), a middle metagreywacke series (metaturbidites, Armina Formation), and

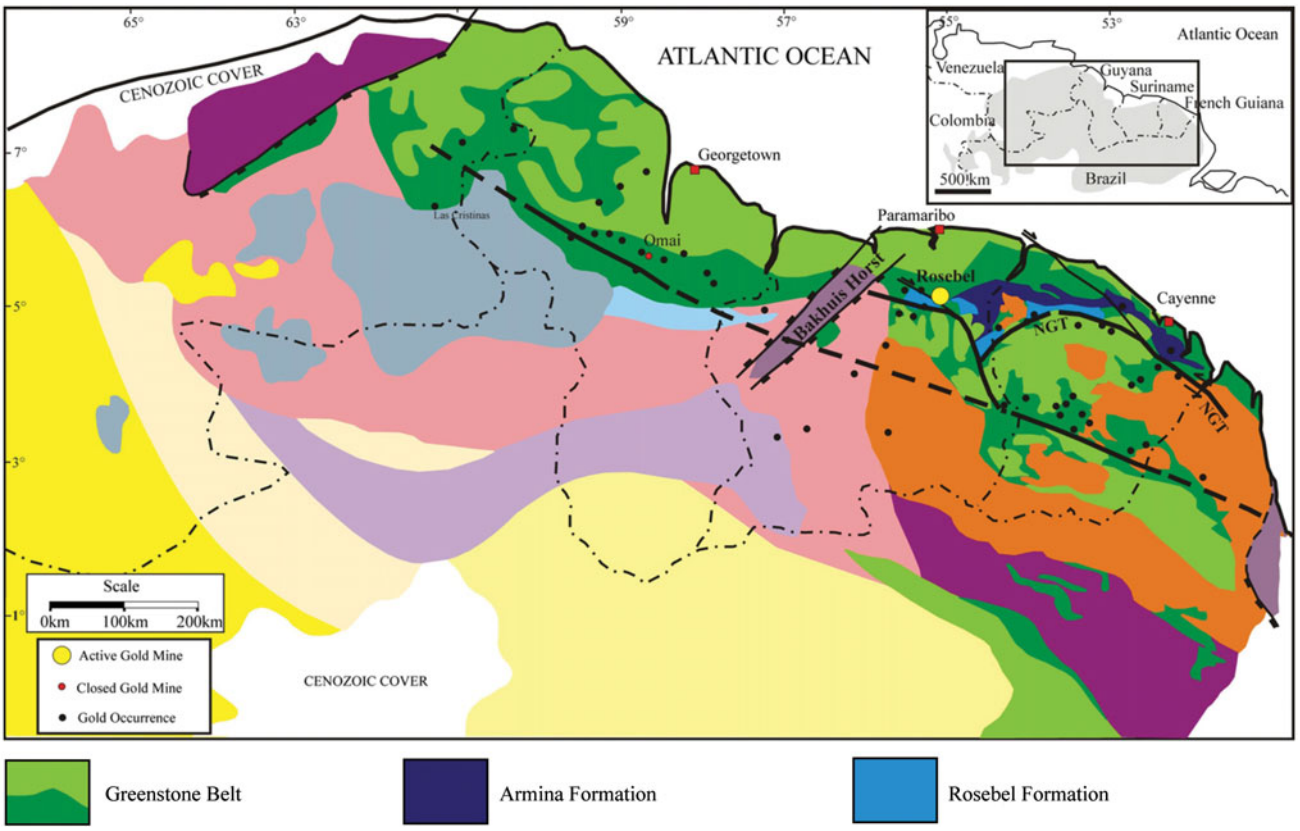

Fig. 1. Simplified geology of the northern Guiana Shield with the Greenstone belt, Armina Formation and Rosebel Formation. Modified after Daoust et al. (2011) (see there for other legend units).

an upper series of epicontinental meta-arenites and metaconglomerates (Rosebel Formation) (Fig. 2). The tholeiitic character of the lowermost mafic volcanics suggests an ocean floor or back-arc basin origin, and the calc-alkaline character of the remainder of the volcanics is in harmony with a volcanic arc origin (Vanderhaeghe et al., 1998; Delor et al., 2003a,b). The greenstone belt has been metamorphosed under greenschist and locally amphibolite-facies conditions, and has been intruded by diapiric tonalite–trondhjemite–granodiorite (TTG) bodies resulting from subduction of ocean crust (Delor et al., 2003a) and by younger biotite and muscovite granite plutons (Bosma et al., 1983). The main orogenic event that formed and deformed the greenstone belt is the Trans-Amazonian Orogenic Cycle as defined by Hurley et al. (1967), now considered to be due to subduction and subsequent collision of the Amazonian Craton with the West-African craton between 2.2 and 1.9 Ga (Delor et al., 2003a,b). Late deformation events gave rise to the development of extensive gold mineralisation in several generations of quartz veins (Daoust et al., 2011).

Study area

The Armina Formation is exposed mostly in northeastern Suriname and consists of low-grade metamorphic turbidite sequences with centimetre-scale alternations of metagreywacke, phyllite and/or schists and some quartzites. It was deformed and metamorphosed during the Paleoproterozoic Trans-Amazonian Orogenic Event, and intruded by bi-mica and biotite granite bodies (De Vletter, 1984). It continues into French Guiana, where it is known as Bonidoro Group (Marot & Capdevila, 1980; Delor et al., 2003a; Daoust et al., 2011). Most data from this area were collected during expeditions in the early 20th century (IJzerman, 1931) and during the 1950s by the Geological and Mining Service of Suriname (GMD), published as the 1:100,000 sheets Java (De Munck, 1954a), Bigiston (De Munck, 1954b) and Nassau (De Munck, 1954c), and during later fieldwork by GMD in the 1970s. The turbiditic character of the Armina Formation was recognised by Bosma & Groeneweg (1970), who called it 'flysch-type sedimentation', and was later confirmed by Bosma et al. (1983) and De Vletter (1984). Metamorphism is restricted to greenschist facies conditions (chlorite or biotite subfacies). Due to the dense rainforest vegetation and deep chemical weathering, contacts with the underlying and overlying formations are nowhere exposed, but the cumulative thickness is at least 1000 m (Daoust et al., 2011). The Armina Formation is supposed to be overlain by the Rosebel Formation with an unconformity, but the distinction between the two formations is sometimes difficult, a point that will also be addressed in this paper. The Armina Formation is strongly folded

https://doi.org/10.1017/njg.2016.9 Published online by Cambridge University Press

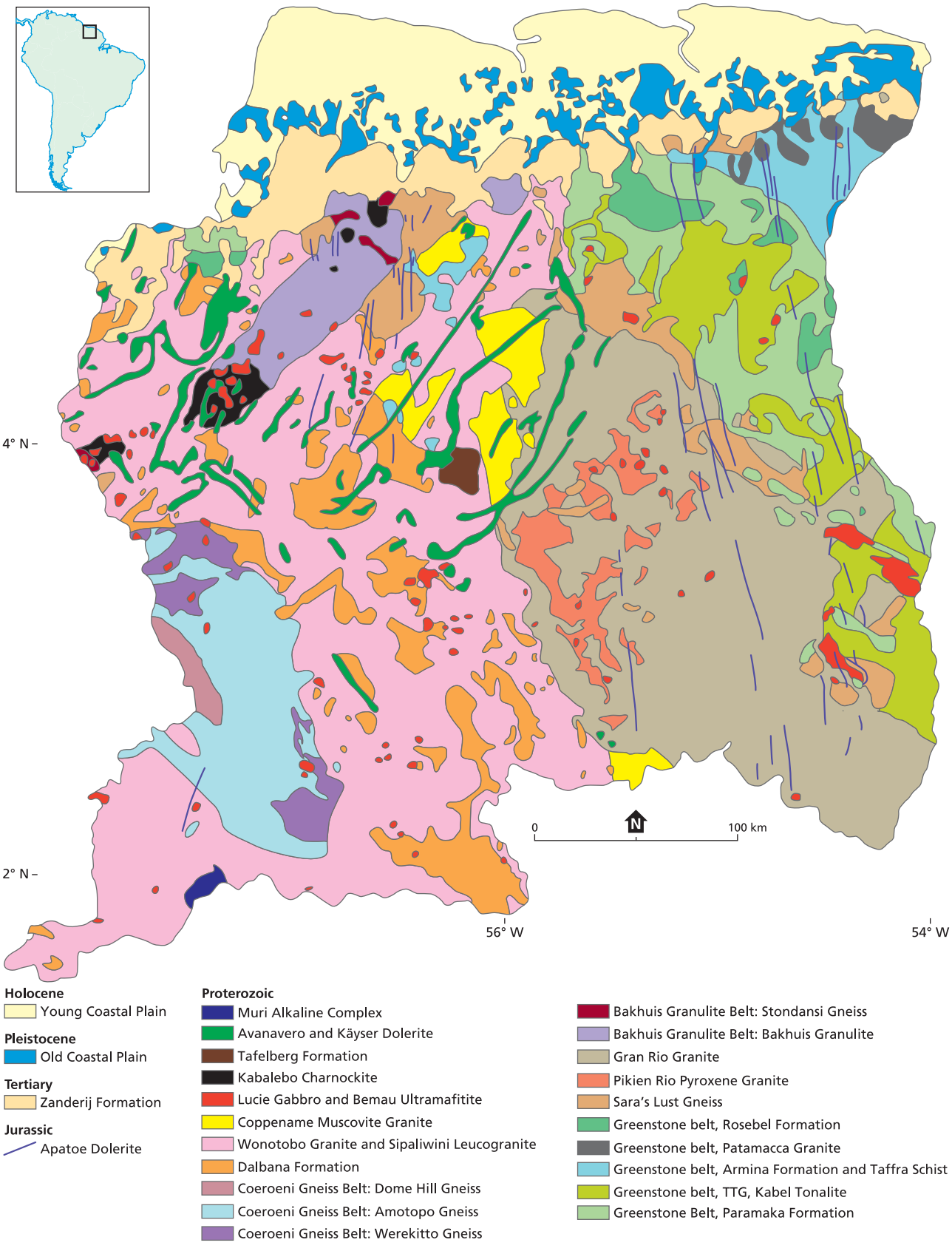

Fig. 2. Geological map of Suriname (Kroonenberg et al., 2016).

https://doi.org/10.1017/njg.2016.9 Published online by Cambridge University Press

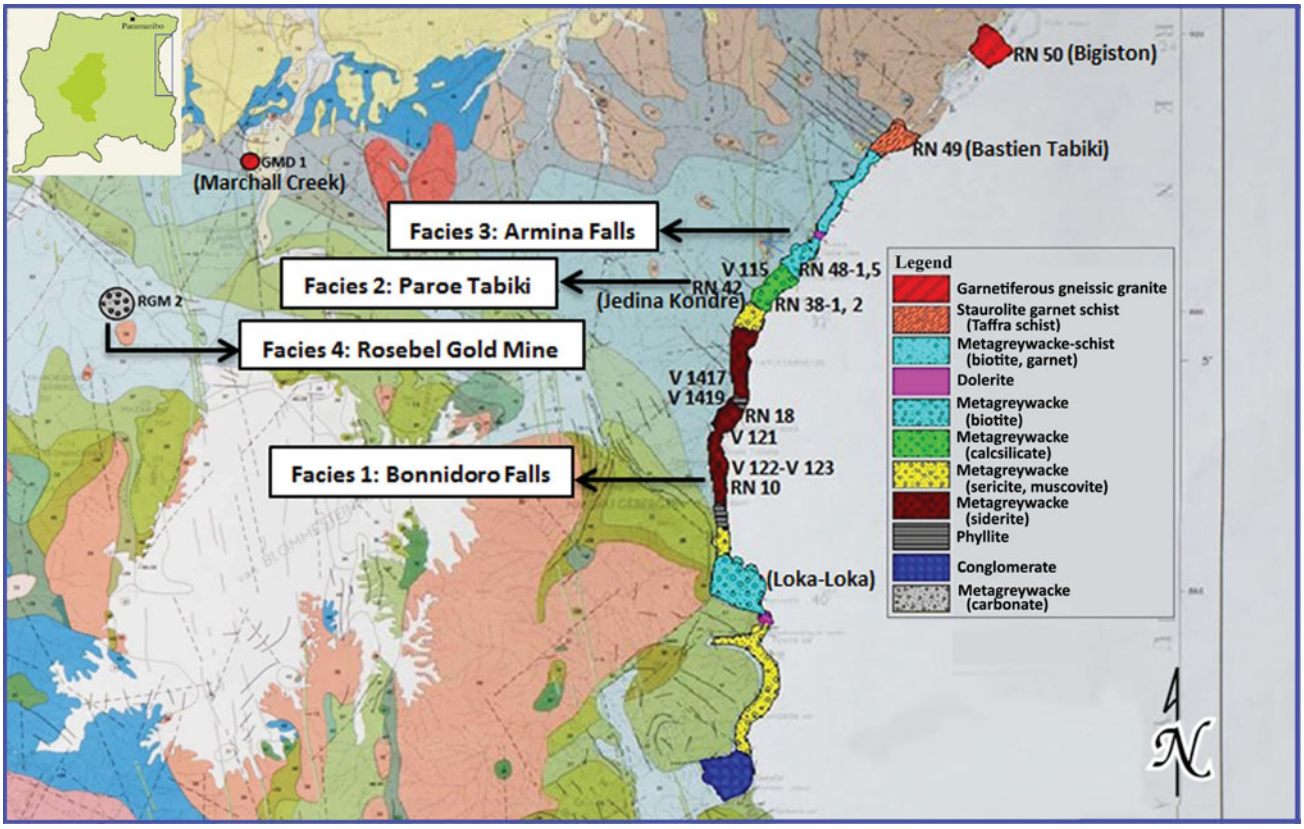

Fig. 3. A general geological map of the sampling route, Marowijne River and the four different metagreywacke facies of the Armina Formation modified from Bosma et al. (1977).

with a generally NW–SE strike. No direct geochronological data are available, but in adjacent French Guiana the underlying tholeiitic lavas of the Paramaka Formation have been dated between 2.156 and 2.137 Ga, the associated TTG plutons 2.18–2.13 Ga, while detrital zircons from the overlying Rosebel Formation show ages around 2.115 Ga (Delor et al., 2003a; Daoust et al., 2011).

Data acquisition and methodology

Data were collected from two different areas. Fieldwork was carried out along the Marowijne River in eastern Suriname that forms the border between French Guiana and Suriname. Several outcrops over a distance of 100 km from Loka-Loka (south) to Bigiston (north) were described and sampled. The most extensive outcrops are at the Bonnidoro Falls, Paroe Tabiki and Armina Falls (Fig. 3).

Turbidite sequences were logged and their sedimentary structures such as graded bedding, convolute lamination and climbing ripples were described. The coarsest rocks are coarse sandy greywackes, the finest beds consist of phyllites. Bedding planes have a general orientation of 75–170°, schistosity is sometimes parallel, sometimes at an angle to the bedding planes (140–170°), dipping subvertically to vertically, 75–90°. The second study area is the Rosebel Gold Mine (RGM) south of Paramaribo, some 100 km west of the Marowijne River outcrops. Drill cores from the JZone pit in the mine were logged and sampled at the core shack of the RGM.

All samples were cut in two with a diamond blade. Half of the samples were pulverised in a ball mill and homogenised in a cone splitter by FILAB in Paramaribo. The prepared samples were analysed with X-ray fluorescence (XRF) for major elements in the ALS Environmental Laboratory in Lima, Peru. No trace elements were analysed. Thin sections were prepared from the other half of the samples at Utrecht University, the Netherlands. Six representative metagraywacke thin sections out of 19 were selected for point counting, as well as eight thin sections from earlier GMD surveys in the same area, giving 14 point-counted thin sections. Two hundred points were counted in each thin section in a grid of 1.5 × 2 mm. Only sand grains between 0.63 mm and 3 mm were counted, using the Gazzi–Dickinson point-counting technique (Dickinson, 1970). All grains were counted as individual mineral grains regardless of whether they occur as free clasts or in rock fragments.

https://doi.org/10.1017/njg.2016.9 Published online by Cambridge University Press

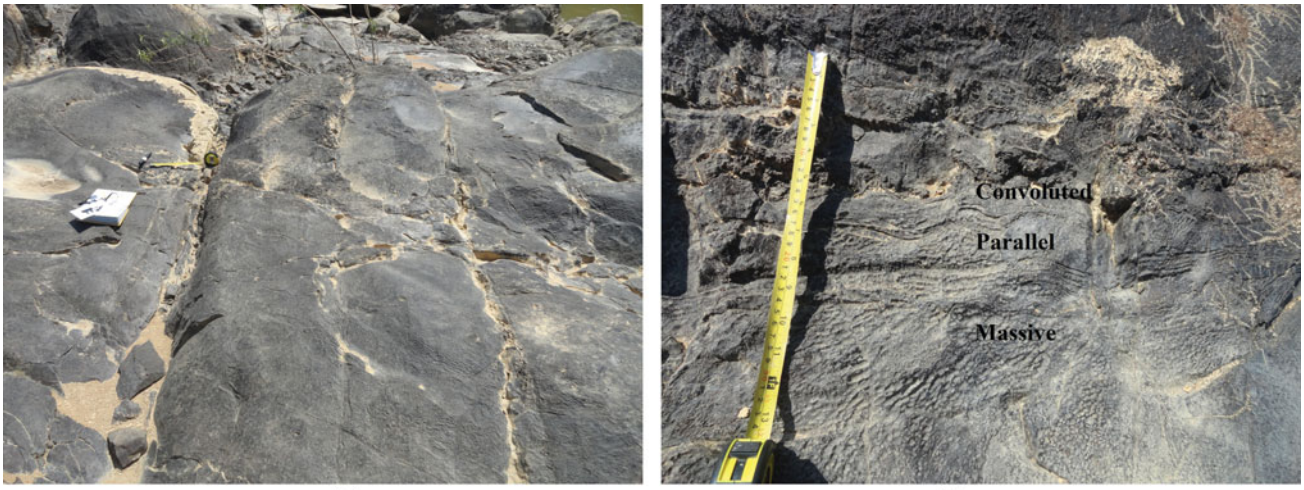

Fig. 4. A. The turbidite outcrop of the Bonnidoro Falls; B. Close-up view of the three different beds of the turbidites from the Bonnidoro Falls.

Sand-sized grains resulting from metamorphism (e.g. garnet, biotite) were not counted.

Field data

Field, petrographic and geochemical data allowed the recognition of four different turbidite facies, three in the Marowijne area and one in the RGM.

Facies 1: Bonnidoro Turbidites. A sequence of about 18 m of turbidites (Fig. 4a) was described from the Bonnidoro Falls. Each turbidite unit consists of three repeating beds (Fig. 4b):

(a) Massive, dark-light grey, well-indurated, poorly sorted greywacke containing abundant medium- to coarse-grained, angular to sub-rounded quartz, feldspar and some rock fragments. This unit shows slight grading. The average thickness of an individual massive greywacke bed is approximately 1.6 m.
(b) Thin, less-competent phyllite beds approximately 0.1 m thick with visible sedimentary structures like convolutions, cross-bedding and climbing ripples. The climb and stoss side angles are both 30° (Fig. 5), which means these are critically climbing ripples with a general orientation of S 10° E (cf. Hunter, 1977).
(c) The upper part of a sequence consists of thin parallel-laminated layers; these are also less competent and finely laminated with an average thickness of 7 cm. A schematic view of the turbidite sequences is given in Fig. 6.

Facies 2: Paroe Tabiki turbidites. In outcrops between Jedina Kondre and south of the Armina Falls typical greenish greywackes occur which differ from the greywacke found elsewhere in the research area. The turbidites of the Paroe Tabiki are comparatively thin beds of approximately 0.3 m in thickness.

Fig. 5. Climbing ripples in the convoluted layers of the turbidites from the Bonnidoro Falls.

The sequence consists of two repeating lithological associations (Fig. 7):

(a) Massive, dark-grey, well-indurated, poorly sorted greywacke containing abundant medium- to coarse-grained, angular to sub-rounded quartz, feldspar and some rock fragments. This unit shows slight grading. The average thickness of an individual massive greywacke bed is approximately 0.2 m.
(b) Alternating thin-bedded schistose sequences: poorly indurated, fine-grained, schistose beds with an average thickness of 0.1 m. A schematic view of the turbidite sequences

https://doi.org/10.1017/njg.2016.9 Published online by Cambridge University Press

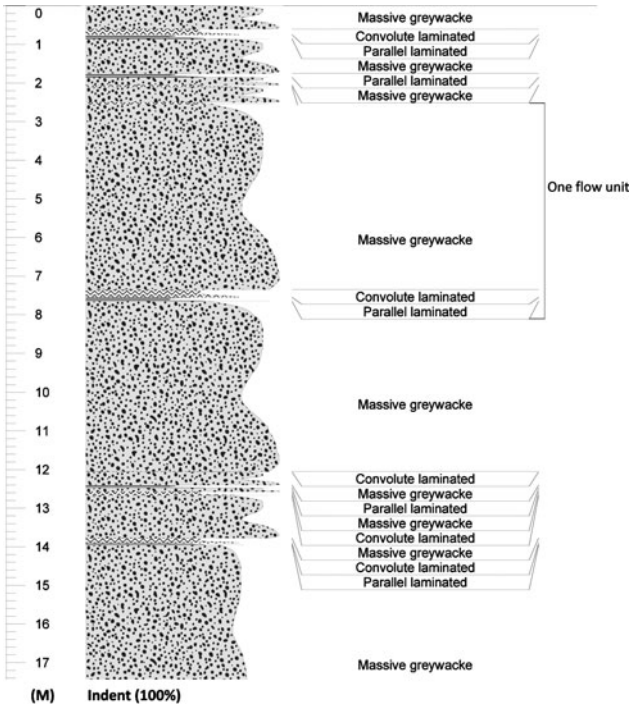

Fig. 6. Schematic view of the turbidite sequences of the Bonnidoro Falls: the x-axis is outcrop relief (proxy for grain size) and the y-axis is thickness of the layers (m).

Fig. 7. The three repeating beds of the Paroe Tabiki.

is given in Fig. 8. This unit contains numerous concentric calcsilicate concretions up to 10 cm in diameter. They are often hollow inside, likely due to dissolution of carbonate (Fig. 9). The bedding planes wrap around the concretions, suggesting that the concretions were formed diagenetically in the soft greywackes.

Facies 3: Turbidites of the Armina Falls. Here a sequence of turbidites (Fig. 10a) is exposed over 15 m, consisting of five distinguishable beds (Fig. 10b): massive, coarse-grained greywacke, grey, well-indurated, poorly sorted greywacke with abundant medium to coarse, angular to sub-rounded quartz and

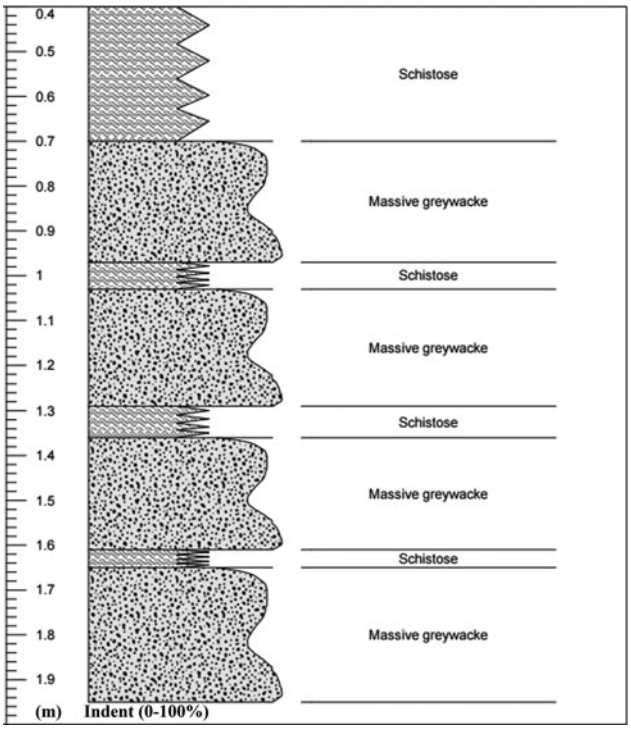

Fig. 8. Schistose of the turbidite sequences of the Paroe Tabiki Falls: the x-axis is outcrop relief (proxy for grain size) and the y-axis is thickness of the layers (m).

feldspar CLASTS with some rock fragments and biotite porphyroblasts. (a) An individual, massive, coarse-grained greywacke 0.7 m thick; (b) massive medium- to fine-grained greywacke beds approximately 0.3 m thick; (c) a parallel-laminated phyllitic bed and (d) phylllitic beds with convolute laminations, greenish grey, fine-grained with an average thickness of 0.1–0.2 m. (e) The schistose layers are greenish grey, very fine-grained, shimmery and foliated, with a few biotite and opaque porphyroblasts. The average thickness of these layers is about 0.1 m. Fig. 11 gives a schematic view of the five units.

Facies 4: Turbidites of the RGM area. The sequences in the RGM area consist of (1) rhythmic alternations of light and dark thinly laminated phyllite, (2) graded, greenish-grey and coarse-grained greywacke beds 0.3–0.4m thick, locally with scours at the bottom, and (3) a 4.4-m thick polymict conglomerate with elongated pebbles (Figs 12a,b and 13).

Petrography

General characteristics

The fine- to coarse-grained metagreywackes consist predominantly of quartz and feldspar in a matrix of quartz and sericite. At some places carbonate, chlorite and/or biotite are also present. The metagreywackes in the Marowijne River Area are

https://doi.org/10.1017/njg.2016.9 Published online by Cambridge University Press

Fig. 9. The calcsilicate concretions in the green turbidites.

generally poorly sorted, texturally sub-mature (cf. Folk, 1951), with sub-angular to sub-rounded clasts, and mineralogically immature (cf. Pettijohn et al., 1972; Blatt et al., 1980; Herron, 1988). They contain monomineralic quartz and feldspar clasts of 0.5–3.5 mm. Quartz occurs as monocrystalline and polycrystalline clasts, as veins, matrix cement and grains in rock fragments. Some quartz clasts contain embayments (Fig. 14a), typical for quartz phenocrysts of volcanic (rhyolitic) origin. The feldspar occurs as clasts as part of plutonic rock fragments. The feldspar group is dominated by plagioclase and only a few alkalifeldspar clasts were counted. Sericitization is common (Fig. 14b), and plagioclase clasts are often saussuritised (Fig. 14c) and locally show myrmekitic intergrowths with quartz (Fig. 14d).

The lithic fragments in the metagreywackes consist of very fine-grained, mafic volcanic fragments (Fig. 15a) and felsic plutonic fragments. The plutonic fragments are probably tonalites (Fig. 15b), composed of quartz, plagioclase laths and sericite grains. The largest plutonic clast counted is 3 mm, while the volcanic clasts range from 0.35 to 2 mm. Other rock fragments are quartzite, counted as quartz in the QFL diagrams and as rock fragments in the QmFLt diagrams (cf. Ingersoll et al., 1984), and phyllite. The matrix consists of sericite, quartz, chlorite, epidote and carbonate. Zircon, opaque minerals and tourmaline are common accessory minerals.

Distinguishing characteristics of the four facies

Facies 1. Both metagreywackes and metapelites of facies 1 contain well-rounded 0.1–2 mm, orange–red poikiloblasts of probably oxidised siderite, which react strongly with HCl (Fig. 16a–c). The carbonate is often only present as rhombohedral skeletal remains around pelitic inclusions. They were probably formed during diagenesis or early metamorphism in the pelitic sediments, as they include finer-grained pelitic material than outside the poikiloblasts, and appear to have rotated during metamorphism (Fig. 16d).

Facies 2: The green metagreywacke of facies 2, between Jedina Kondre and Kalfoe Kondre south of the Armina Falls, is very rich in quartz and contains feldspar, phyllite fragments, chlorite and epidote. The green colour is explained by the presence of typical green minerals like chlorite and epidote. The concentric concretions from Jedina Kondre and Paroe Tabiki consist largely of calcsilicate minerals: fan-shaped actinolite (Fig. 17a), biotite, chlorite, garnet poikiloblasts (andradite, a Ca-garnet) (Fig. 17b) with quartz and chlorite inclusions, epidote (Fig. 17c) and clinozoisite (Fig. 17c,d). This mineral association results from a chemical reaction between the original carbonate and the surrounding quartz-rich rocks during metamorphism.

Facies 3: The coarse-grained sample RN 48-1 and the medium-grained massive metagreywacke sample RN 48-2 contain abundant medium to coarse, angular to sub-rounded quartz

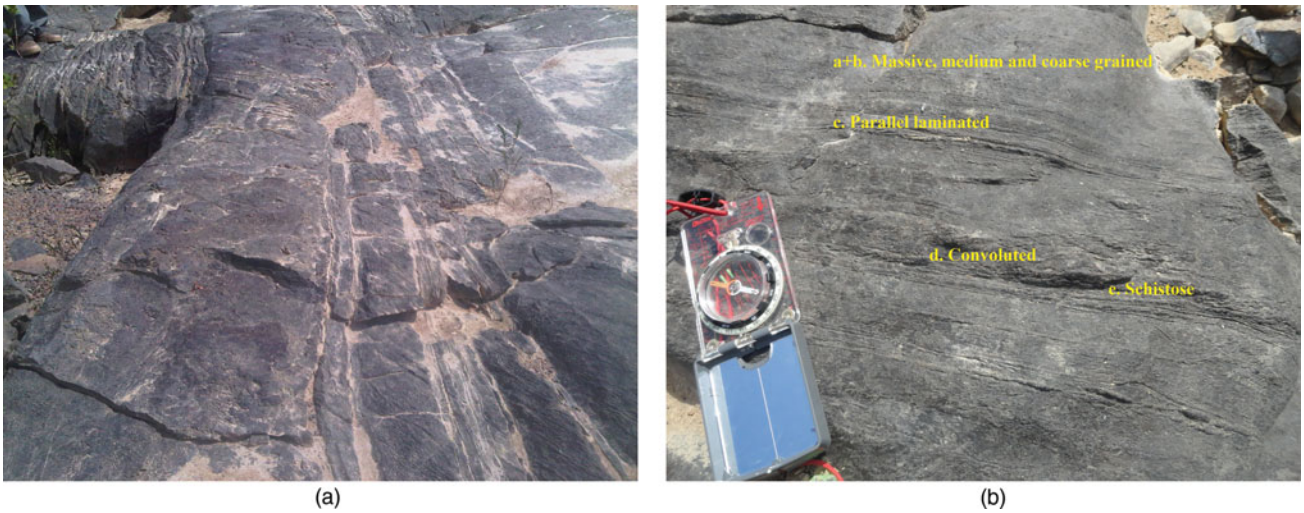

Fig. 10. A. The turbidite outcrop of the Armina Falls. B. Close-up view of the five different beds of the Armina turbidites.

https://doi.org/10.1017/njg.2016.9 Published online by Cambridge University Press

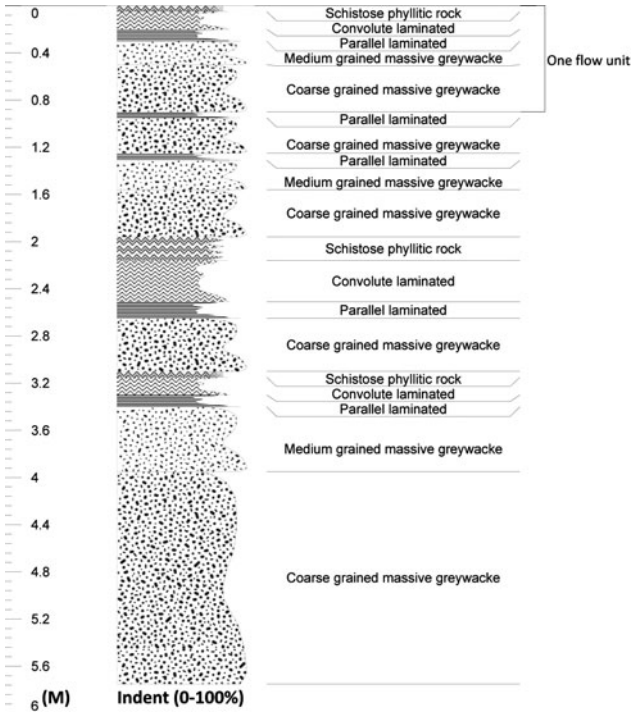

Fig. 11. Schematic view of the turbidite sequences of the Armina Falls: the x-axis is outcrop relief (proxy for grain size) and the y-axis is thickness of the layers (m).

and feldspar clasts, some rock fragments and tabular biotite porphyroblasts (Fig. 18). Thin-bedded laminated sample RN 48-3 and convolute layer sample RN 48-4 contain fine-grained clasts with opaque minerals and biotite porphyroblasts. The schistose layer sample RN 48-5 consists of very fine-grained minerals, and is laminated and schistose, with few biotite and opaque porphyroblasts. The matrix is very rich in quartz and consists further of chlorite, very fine fragments of sericite, some muscovite and porphyroblasts of biotite. Only one sample, RN 48-1, has been point counted because in the finer beds it is impossible to differentiate between the quartz clasts and matrix due to recrystallisation during metamorphism. The presence of biotite indicates a higher grade of metamorphism than in the other three turbidite facies.

Facies 4: The conglomerates of the RGM cores are polymictic, with more lithic fragments than free minerals. The lithic fragments consist of mafic volcanic rocks, fine-grained mafic, porphyritic rocks with feldspar laths and a fine-grained mafic matrix, and further phyllite and quartzite grains. The pebbles are rounded and elongated, evidencing deformation. The matrix is rich in carbonate, quartz and sericite. Other minerals found in the matrix are epidote, calcite and opaque minerals like oxides. The graded metagreywacke in the cores consists of angular quartz clasts of about 0.5 mm, opaque minerals and calcite crystals in a carbonate, sericite and chlorite matrix. The metagreywacke is greenish grey and contains many calcite–quartz micro-veins.

The finely laminated phyllites in the cores are rich in mafic minerals (especially chlorite) in the darker laminae, while the lighter laminae contain fewer mafic minerals.

Point-counting results

The results of all the point-counted thin sections are summarised in Table 1. Table 2 contains further processed data. The data of Table 1 are plotted in the QFL diagram (Fig. 19). Almost all the samples are categorised as feldspathic wacke except for the metagreywacke of a quartz-rich quartzwacke, and a lithic wacke in facies 4 with a high concentration of lithic fragments.

A comparison of the point-counting results of the four different facies clearly shows that the RGM samples are much richer in volcanic clasts, whereas the Marowijne facies are richer in quartz and plagioclase. This suggests that the two study areas may have different provenance areas. The possible

Fig. 12. A. Greenish-grey and coarse-grained greywacke drill cores of RGM. B. Scours at the bottom of the layers in the drill cores of RGM.

https://doi.org/10.1017/njg.2016.9 Published online by Cambridge University Press

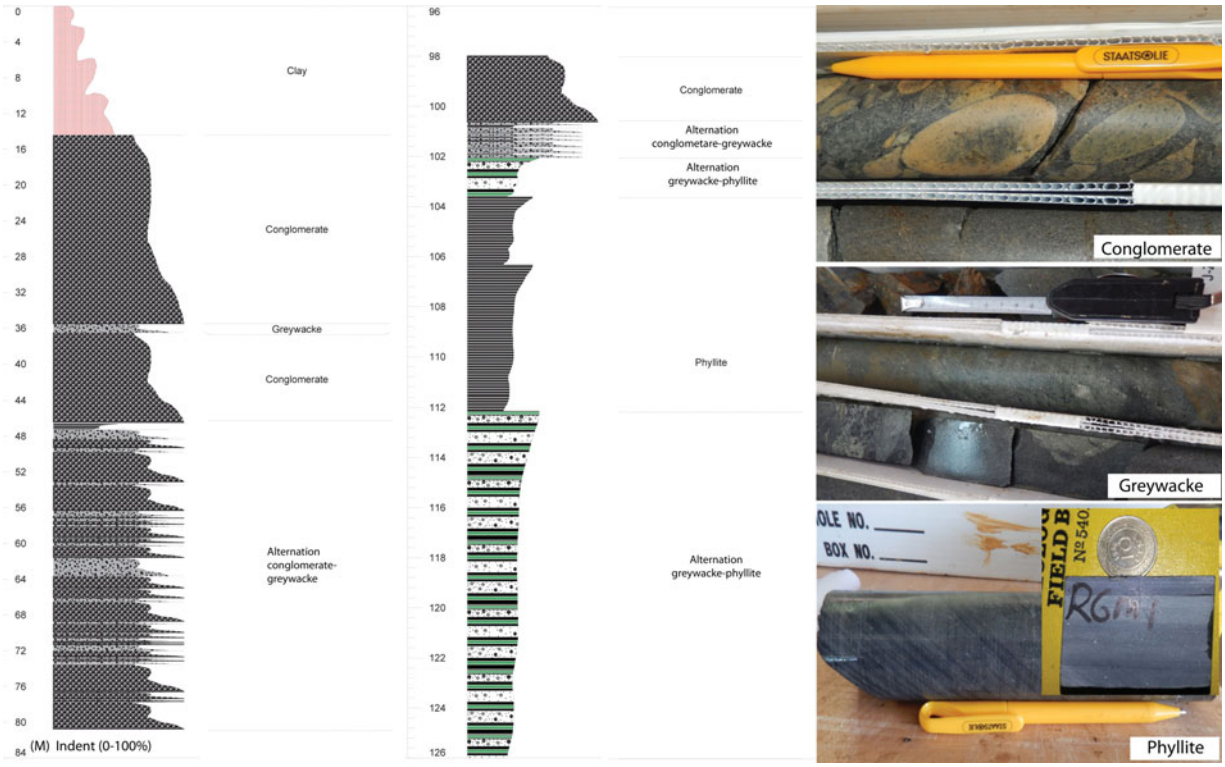

Fig. 13. Schematic view of the turbidite sequences of RGM: the x-axis is outcrop relief (proxy for grain size) and the y-axis is thickness of the layers (m).

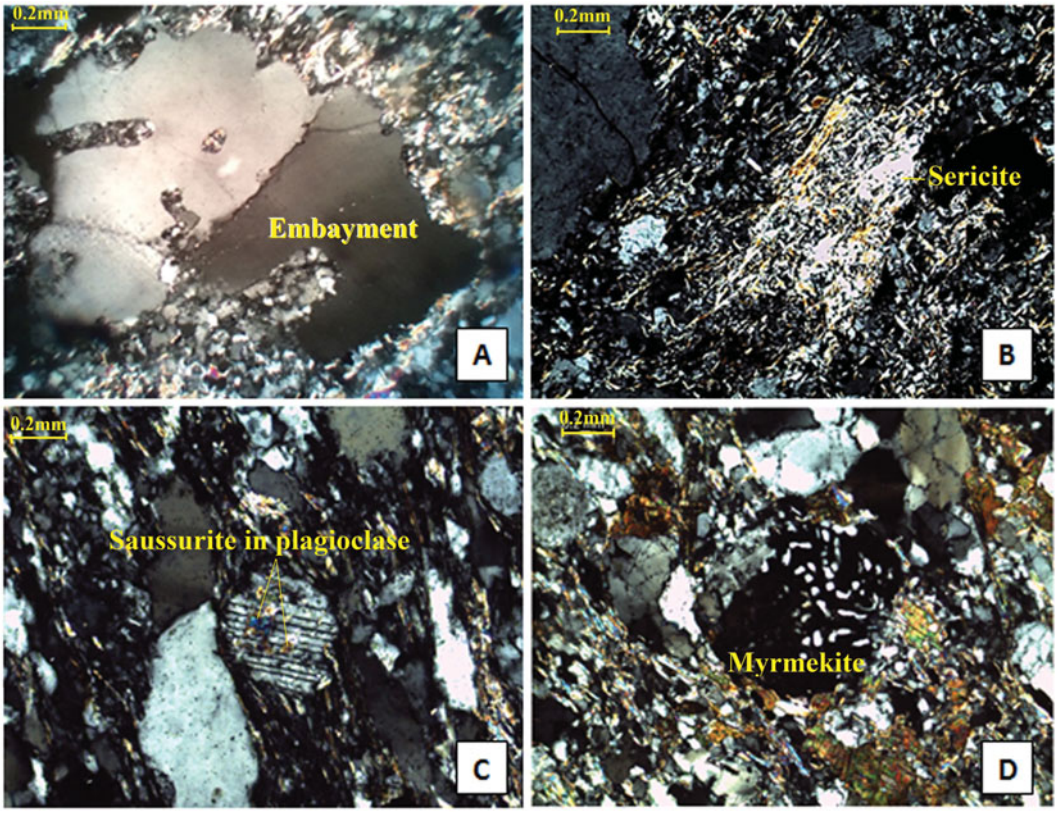

Fig. 14. A. Embayments in the quartz clast (10X, XPL); B. Sericitation of plagioclase (10X, XPL); C. Saussurite in plagioclase (4X, XPL); D. Myrmekite.

https://doi.org/10.1017/njg.2016.9 Published online by Cambridge University Press

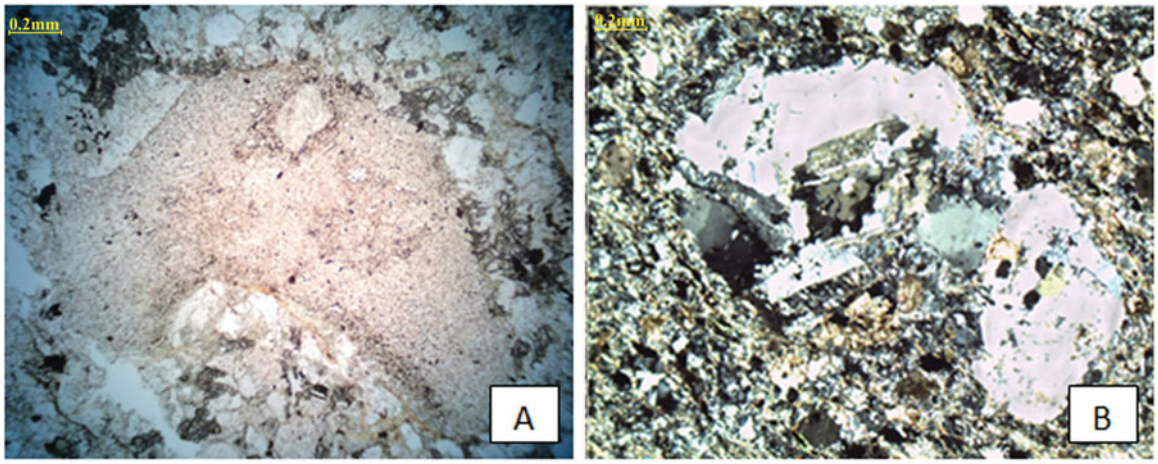

Fig. 15. A. Sub-rounded, fine grained, mafic volcanic clast (10X, PPL); B. Sub-rounded, felsic plutonic fragments (10X, XPL).

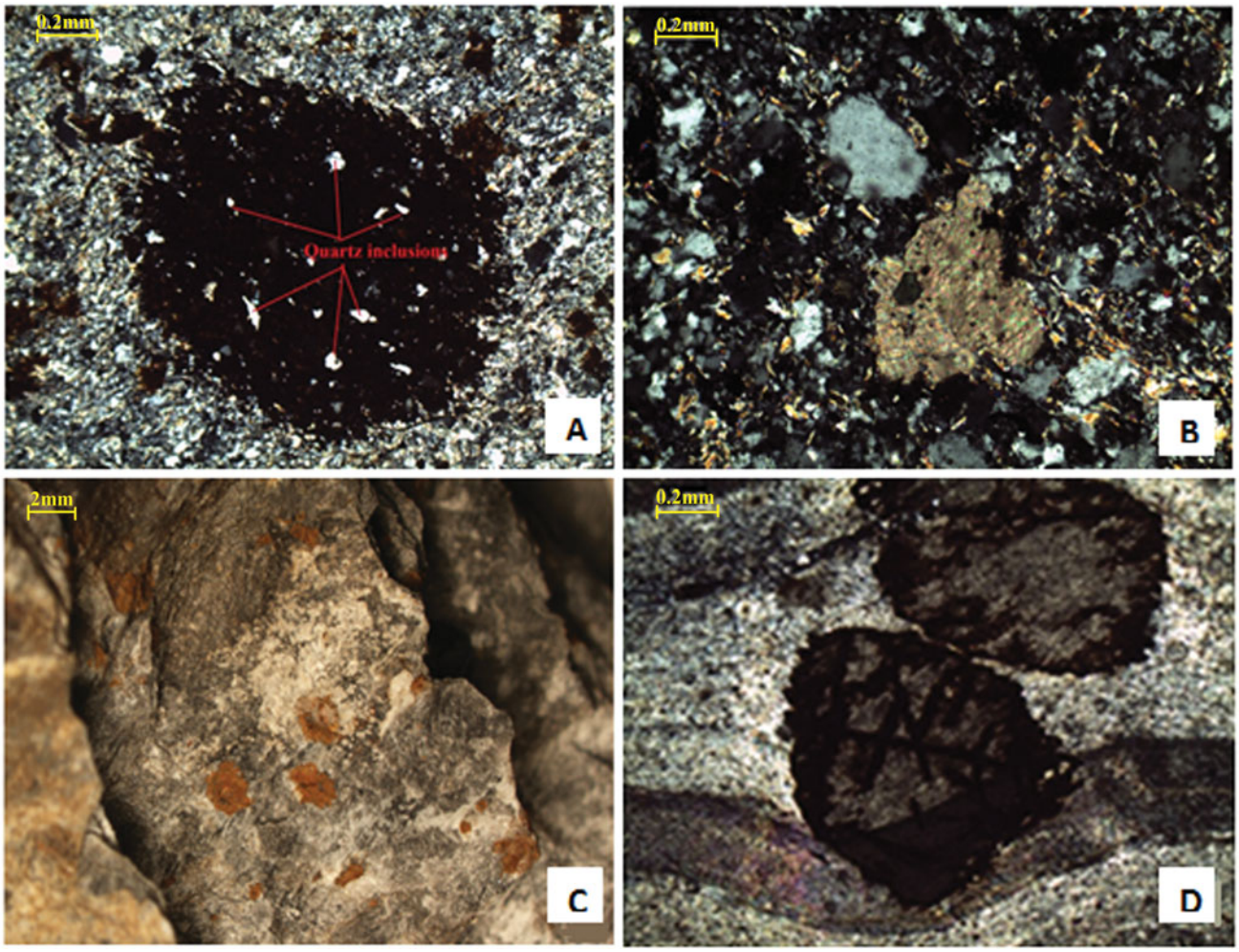

Fig. 16. A. Carbonate poikiloblast in the Bonnidoro metagreywacke with quartz inclusions(4X, XPL); B. Fresh carbonate poikiloblasts in the Bonnidoro metagreywacke (4X, PPL); C. The powder substance disseminated over the phyllite sample with orange porphyroblasts (1X); D. The rotated poikiloblasts in the pelitic matrix, which have a high interference colour, probably due to the presence of carbonate.

https://doi.org/10.1017/njg.2016.9 Published online by Cambridge University Press

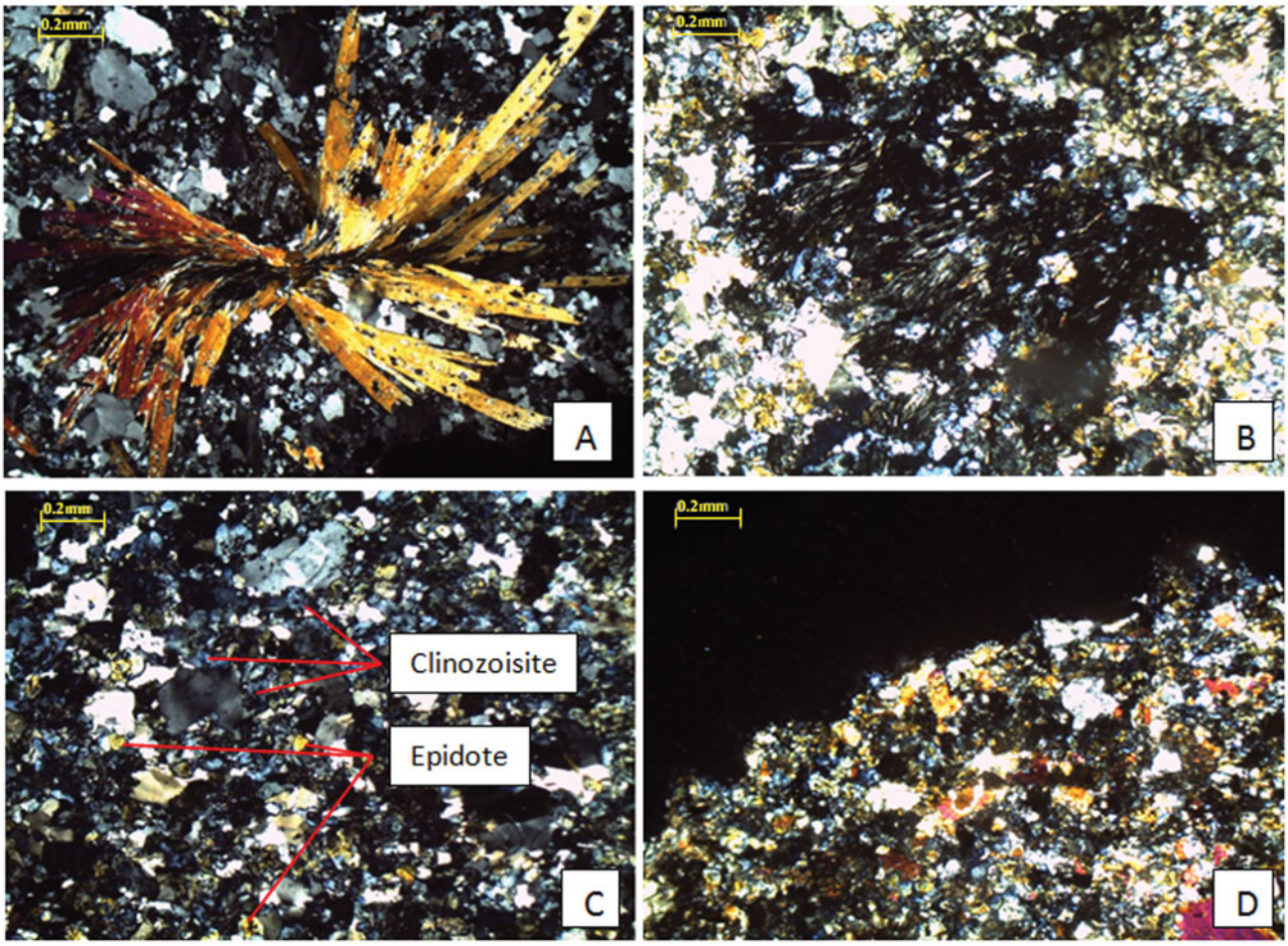

Fig. 17. A. Actinoline (10X, XPL); B. Formation of garnet surrounded by epidote and clinozoisite (10X, XPL); C. Clinozoisite and epidote in a quartz matrix (10X, XPL); D. Concentration of epidote and clinozoisite near the core of the concretion.

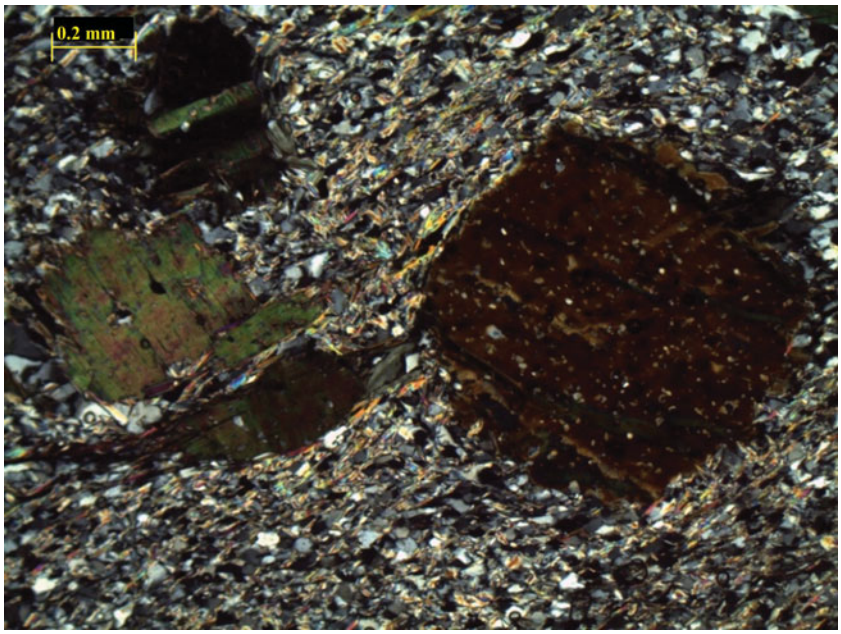

Fig. 18. Biotite porphyroblasts (10X, XPL).

https://doi.org/10.1017/njg.2016.9 Published online by Cambridge University Press

Table 1. Data from point counting for QFL diagram.

		Raw point-counted data (%)					Total without	Normalised point-counted data (%)			Average (%)		
Sample no.	Location	Quartz	Feldspar	Lithic	Matrix	Total	matrix	Q	F	L	Q	F	L
V121	Facies 1: Bonnidoro Falls	30.0	18.5	10.7	40.7	100.0	59.3	50.7	31.3	18.1	56.3	25.8	17.8
V122	Facies 1: Bonnidoro Falls	29.4	17.9	11.9	40.8	100.0	59.2	49.6	30.3	20.2			
V123	Facies 1: Bonnidoro Falls	32.1	19.2	9.6	39.1	100.0	60.9	52.6	31.6	15.8			
V124	Facies 1: Bonnidoro Falls	34.0	21.0	13.5	31.5	100.0	68.5	49.6	30.7	19.7			
V1417	Facies 1: Bonnidoro Falls	38.8	12.4	10.9	37.8	100.0	62.2	62.4	20.0	17.6			
V1419	Facies 1: Bonnidoro Falls	40.6	15.1	13.7	30.7	100.0	69.3	58.5	21.8	19.7			
RN10	Facies 1: Bonnidoro Falls	32.7	8.7	8.0	50.7	100.0	49.3	66.2	17.6	16.2			
RN18	Facies 1: Bonnidoro Falls	30.8	11.9	7.7	49.7	100.0	50.3	61.1	23.6	15.3			
RN48-1	Facies 2: Armina Falls	42.2	1.9	0.5	55.3	100.0	44.7	94.6	4.3	1.1	58.7	4.3	37.0
V115	Facies 3: Paroe Tabiki	40.5	11.5	4.0	44.0	100.0	56.0	72.3	20.5	7.1	74.3	19.8	5.9
RN38-1	Facies 3: Paroe Tabiki	46.6	11.3	3.4	38.7	100.0	61.3	76.0	18.4	5.6			
RN38-2	Facies 3: Paroe Tabiki	43.7	11.9	3.0	41.4	100.0	58.6	74.6	20.3	5.1			
RGM2	Facies 4: RGM	29.0	4.0	16.0	51.0	100.0	49.0	59.2	8.2	32.7	59.2	8.2	32.7

Q, total quartzose grains (mono- and polycrystalline), including lithic fragments such as chert and quartzite; F, feldspar; L, unstable, lithic grains (rock fragments).

Table 2. Data from point counting for the QmFLt diagram.

		Raw point-counted data (%)					Total without	Normalised point-counted data (%)			Average (%)		
Sample no.	Location	Quartz	Feldspar	Lithic	Matrix	Total	matrix	Qm	F	Lt	Qm	F	Lt
V121	Facies 1: Bonnidoro Falls	24.3	18.5	16.5	40.7	100.0	59.3	41.0	31.3	27.8	45.7	25.8	28.4
V122	Facies 1: Bonnidoro Falls	21.9	17.9	19.4	40.8	100.0	59.2	37.0	30.3	32.8			
V123	Facies 1: Bonnidoro Falls	25.6	19.2	16.0	39.1	100.0	60.9	42.1	31.6	26.3			
V124	Facies 1: Bonnidoro Falls	31.0	21.0	16.5	31.5	100.0	68.5	45.3	30.7	24.1			
V1417	Facies 1: Bonnidoro Falls	30.3	12.4	19.4	37.8	100.0	62.2	48.8	20.0	31.2			
V1419	Facies 1: Bonnidoro Falls	31.1	15.1	23.1	30.7	100.0	69.3	44.9	21.8	33.3			
RN10	Facies 1: Bonnidoro Falls	26.0	8.7	14.7	50.7	100.0	49.3	52.7	17.6	29.7			
RN18	Facies 1: Bonnidoro Falls	27.3	11.9	11.2	49.7	100.0	50.3	54.2	23.6	22.2			
RN48-1	Facies 2: Armina Falls	26.2	1.9	16.5	55.3	100.0	44.7	58.7	4.3	37.0	58.7	4.3	37.0
V115	Facies 3: Paroe Tabiki	24.5	11.5	20.0	44.0	100.0	56.0	43.8	20.5	35.7	50.1	19.8	30.1
RN38-1	Facies 3: Paroe Tabiki	33.8	11.3	16.2	38.7	100.0	61.3	55.2	18.4	26.4			
RN38-2	Facies 3: Paroe Tabiki	30.1	11.9	16.6	41.4	100.0	58.6	51.4	20.3	28.2			
RGM2	Facies 4: RGM	11.0	4.0	34.0	51.0	100.0	49.0	22.4	8.2	69.4	22.4	8.2	69.4

Qm, monocrystalline quartz; F, feldspar grains; Lt, total polycrystalline lithic fragments, including quartzose varieties.

https://doi.org/10.1017/njg.2016.9 Published online by Cambridge University Press

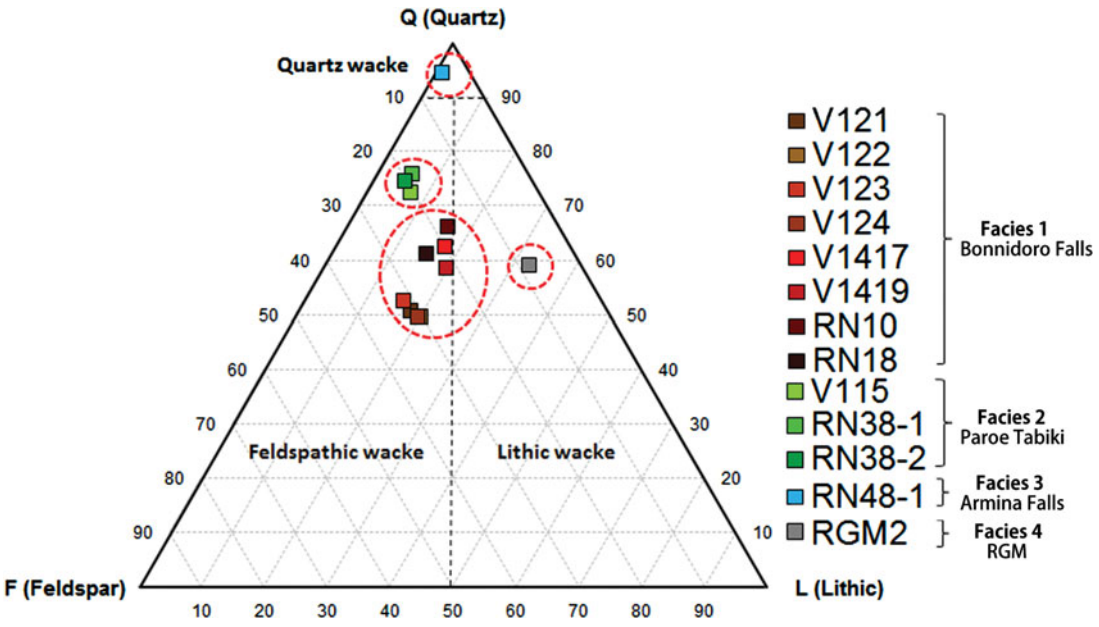

Fig. 19. A QFL diagram showing the mineral composition of the four facies.

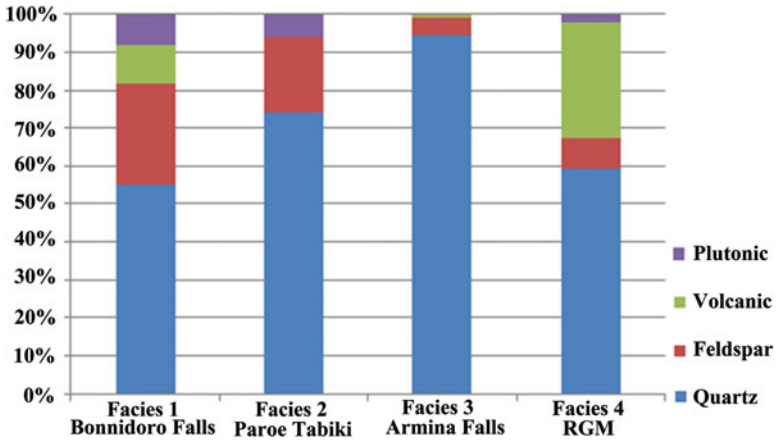

Fig. 20. A column diagram of the greywacke clasts of the Marowijne River and RGM.

stratigraphic and chronological implications are discussed below (Fig. 20).

Relationship between petrographic composition and tectonic setting

The tectonic provenance discriminating diagrams QFL and QmFLt (cf. Dickinson et al., 1983) provide information about the tectonic settings of the associated provenance areas and the basins of deposition by modal percentage calculation. The point-counting data are summarised in Table 2 and plotted in the QmFLt triangle diagrams (Fig. 21).

These diagrams show that the comparatively high polycrystalline quartz and quartzite content of the rocks drags the samples into the mixed-dissected arcs and quartzose recycled category when the quartz is grouped with the lithic fragments (diagram on the right). The provenance is therefore more likely to be recycled orogenic than magmatic arc. The Armina Falls greywacke has a total quartzose framework mode, apparently composed of derivatives of the stable parts of the craton. The Paroe Tabiki samples are slightly more feldspathic, characteristic of the transitional group derived from the continental blocks. The source areas of the Paroe Tabiki suites had probably slightly greater relief than the cratonic provenance, but not enough to produce more feldspathic greywacke. The greywackes in the recycled orogenic block contain lithic fragments which may have been derived from rocks overlying the basement, local volcanic fields that may be related to rifting events or belts of metamorphic rocks associated with basement terranes. This is in harmony with the supposed tonalitic provenance derived from clast petrography. The RGM greywacke is of recycled orogenic and/or recycled lithic provenance. Reading 'lithic' as volcanic, this fits the more volcaniclastic nature of these greywackes.

https://doi.org/10.1017/njg.2016.9 Published online by Cambridge University Press

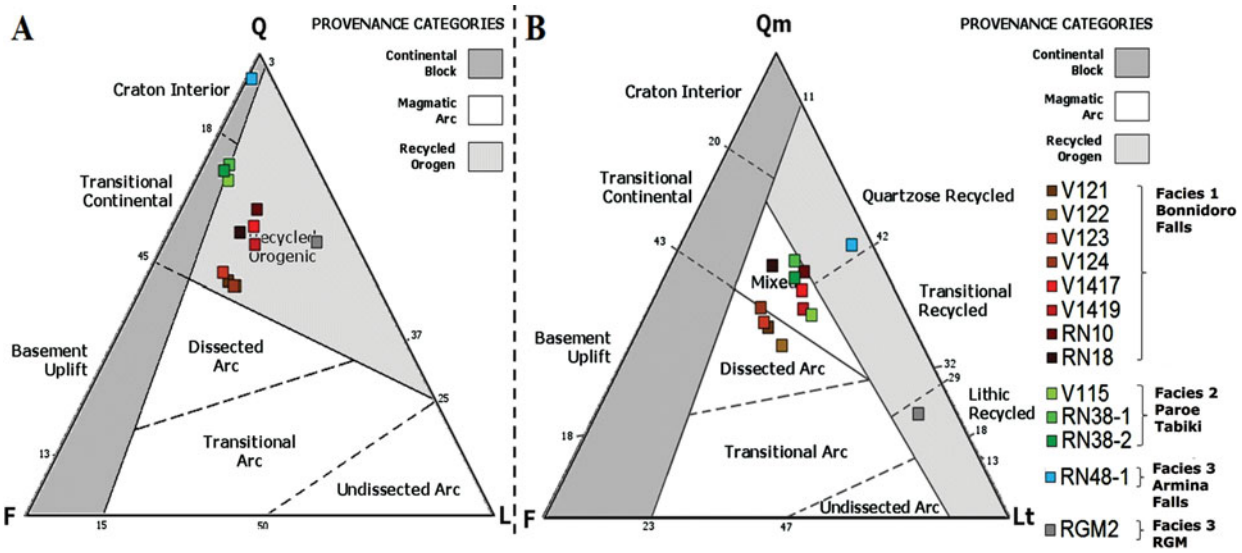

Fig. 21. A. QFL ternary diagram of the metagreywacke from the Marowijne River and one of the RGM (J-Zone), with recycled orogenic, craton interior and transitional continental provenances (Dickinson et al., 1983). B. QmFLt ternary diagram of the metagreywacke from the Marowijne River and one of the RGM (JZone), with mixed-dissected arc, recycled quartzose and recycled lithic provenances (Dickinson et al., 1983).

Geochemistry

Major element data from the four facies

Major element data are summarised in Table 3 and plotted in the log (Na_2O/K_2O) versus log (SiO_2/Al_2O_3) diagram of Pettijohn et al. (1972), together with reference concentrations of post-Archean Australian average shales (PAAS) (Taylor & McLennan, 1985) and upper continental crust (UCC) (Rudnick & Gao, 2003) (Table 3, Fig. 22).

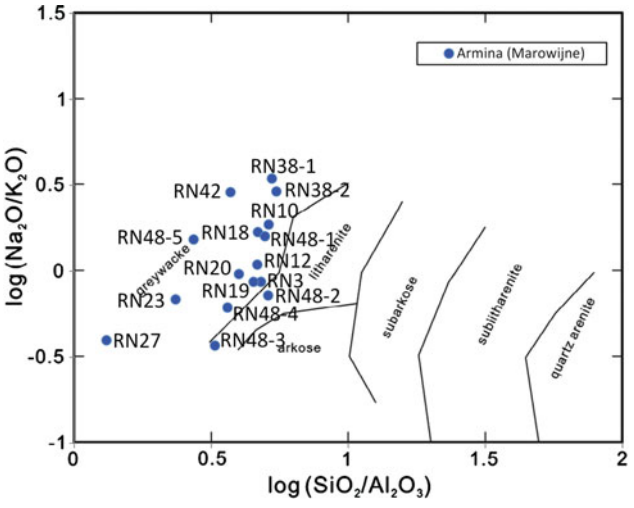

Fig. 22. Classification of the analysed Armina Formation metasedimentary rock samples from the Marowijne River according to their logarithmic ratios of SiO_2/Al_2O_3 and Na_2O/K_2O after Pettijohn et al. (1972).

All samples plot as greywacke except for RN48-2 and RN 48-3. These plot as litharenite. Coarser rocks are usually higher in SiO_2 and lower in Al_2O_3 than finer rocks from the same turbidite unit, as is seen in RN48 1–5: this is the geochemical expression of upwards increasing clay content. The phyllites RN 23 and RN 27 have low SiO_2, MgO and CaO, and high Al_2O_3. The calcsilicate rock RN 42 has high CaO, low Na_2O and K_2O, and has a low K_2O/Na_2O. The four facies do not differ much in their major element distribution, as grain size variations within the individual fining upwards sequences in each facies cause more geochemical differentiation than the petrographic differences between the facies.

Comparison with existing data from the RGM

Table 4 shows existing analytical data from Armina Formation samples from cores drilled in the J-Zone pit (Daoust et al., 2011) and in the Koolhoven pit in the RGM (Carlier, 2012). These also plot in the greywacke field in Pettijohn's diagram (Fig. 23). Some are phyllites, but these cannot be distinguished in the log SiO_2/Al_2O_3 and Na_2O/K_2O plot.

Core samples collected by Daoust et al. (2011) and Carlier (2012) from the Pay-Caro, Mayo, Royal Hill and Rosebel pits in the RGM were classified by them as Rosebel Formation arenites. However, the precise stratigraphic relations with the Armina Formation were not visible in the cores. The published major element results of these samples are summarised in Table 5 and plotted in the log (Na_2O/K_2O) versus log (SiO_2/Al_2O_3) diagram (Fig. 24).

The Pettijohn plot of Fig. 24 shows the samples from Roma and Mayo plot as greywacke, those from Pay Caro as greywacke

https://doi.org/10.1017/njg.2016.9 Published online by Cambridge University Press

Table 3. Major elements of the samples from the Marowijne River with the PAAS and UCC values.

Rock type→	Grey	Grey	Grey	Grey	Grey	Grey	Phy	Phy	Grey	Grey	Grey	Grey	Grey	Grey	Grey	Contact	Schist		
wt% ↓	RN3	RN10	RN12	RN18	RN19	RN20	RN23	RN27	RN38-1	RN38-2	RN42	RN48-1	RN48-2	RN48-3	RN48-4	RN48-5	Gmd1	UCC	PAAS
SiO_2	69.99	65.93	70.89	66.72	67.93	66.70	56.83	41.35	71.54	71.81	63.07	67.87	70.90	62.08	62.79	56.32	61.95	66.60	62.80
TiO_2	0.74	0.80	0.76	1.26	0.66	0.76	0.91	1.54	0.60	0.62	0.45	0.75	0.75	0.77	0.77	1.09	0.74	0.64	1.00
Al_2O_3	14.57	12.89	15.24	14.29	15.06	16.74	24.24	31.55	13.61	13.16	16.98	13.67	13.92	19.05	17.35	20.67	18.50	15.40	18.90
Fe_2O_3	6.48	10.43	7.06	9.68	8.25	7.47	9.71	14.25	5.21	5.70	5.31	7.25	6.98	8.31	9.08	9.82	9.47	5.04	7.22
MnO	0.14	1.06	0.24	0.12	0.36	0.14	0.08	0.12	0.11	0.11	0.39	0.15	0.10	0.13	0.12	0.13	0.16	0.10	0.11
MgO	2.50	2.85	0.71	2.17	2.79	1.97	0.97	4.82	1.31	1.83	1.59	2.66	2.07	3.07	2.38	2.73	3.39	2.48	2.20
CaO	1.02	2.13	0.42	1.47	1.75	1.26	0.65	0.68	3.09	2.45	11.33	2.22	1.32	0.89	1.36	2.49	0.76	3.59	1.30
Na_2O	2.16	2.42	2.15	2.81	1.63	2.41	2.51	1.84	3.62	3.38	1.00	3.00	2.05	1.61	2.29	3.94	1.24	3.27	1.20
K_2O	2.48	1.29	1.97	1.66	1.88	2.50	3.65	4.64	1.05	1.16	0.35	1.88	2.84	4.35	3.72	2.57	3.68	2.80	3.70
P_2O_5	0.12	0.15	0.14	0.15	0.14	0.19	0.14	0.22	0.12	0.09	0.33	0.17	0.14	0.13	0.14	0.26	0.18	0.15	0.16
Cr_2O_3	0.05	0.04	0.03	0.04	0.03	0.03	0.03	0.04	0.05	0.05	0.05	0.05	0.05	0.04	0.04	0.05	0.07	0.01	0.02
Al_2O_3/SiO_2	0.21	0.20	0.21	0.21	0.22	0.25	0.43	0.76	0.19	0.18	0.27	0.20	0.20	0.31	0.28	0.37	0.30	0.23	0.30
K_2O/Na_2O	1.15	0.53	0.91	0.59	1.15	1.04	1.46	2.52	0.29	0.34	0.35	0.63	1.38	2.71	1.63	0.65	2.98	0.86	3.08

Table 4. Major elements of the samples of the Armina Formation from RGM, with the J series samples (Daoust et al., 2011) and the LC series samples Carlier (2012).

		wt% →												Al_2O_3/	K_2O/
		Rock type ↓	SiO_2	TiO_2	Al_2O_3	Fe_2O_3	MnO	MgO	CaO	Na_2O	K_2O	P_2O_5	Cr_2O_3	SiO_2	Na_2O
		UCC	66.60	0.64	15.40	5.04	0.10	2.48	3.59	3.27	2.80	0.15	0.01	0.23	0.86
Code	**Formation (Location)**	PAAS	62.80	1.00	18.90	7.22	0.11	2.20	1.30	1.20	3.70	0.16	0.02	0.30	3.08
J118834	Armina (RGM – JZone)	m-s-g	60.16	0.78	19.28	10.30	0.16	2.26	0.39	2.57	1.84	0.16	0.02	0.32	0.72
J118836	Armina (RGM – JZone)	m-s-g	62.06	0.81	18.58	8.69	0.09	2.58	0.85	2.44	1.66	0.09	0.02	0.30	0.68
J118840	Armina (RGM – JZone)	m-s-g	66.65	1.00	14.56	8.81	0.11	1.32	1.30	2.26	1.65	0.14	0.02	0.22	0.73
J118838	Armina (RGM – JZone)	Conglo	63.07	0.83	16.51	8.15	0.21	2.39	2.73	2.16	1.66	0.13	0.02	0.26	0.77
LC010	Armina (RGM – KH)	Grey	64.21	0.87	17.86	8.00	0.09	2.61	2.02	1.51	1.91	0.10	0.03	0.28	1.26
LC011	Armina (RGM – KH)	Silt-mud	59.12	0.90	22.92	9.67	0.05	2.49	0.39	2.50	1.83	0.17	0.02	0.39	0.73
LC012	Armina (RGM – KH)	Silt-mud	59.06	0.95	22.43	10.63	0.10	2.47	0.88	2.34	2.31	0.15	0.03	0.38	0.99
LC013	Armina (RGM – KH)	Silt-mud	58.65	0.94	23.87	10.69	0.06	2.17	0.43	2.61	2.12	0.10	0.03	0.41	0.81
LC014	Armina (RGM – KH)	Silt-mud	56.90	0.89	24.70	9.81	0.07	2.44	0.74	2.67	2.09	0.23	0.02	0.43	0.79
LC015	Armina (RGM – KH)	Grey	64.51	0.79	17.75	8.12	0.10	2.19	1.58	1.78	2.00	0.14	0.03	0.28	1.12
LC016	Armina (RGM – KH)	Grey	69.68	0.76	14.83	7.28	0.09	1.76	2.04	1.72	1.75	0.06	0.05	0.21	1.02
LC018	Armina (RGM – KH)	Silt-mud	58.79	1.01	23.81	10.29	0.09	2.59	0.28	1.73	2.79	0.11	0.03	0.40	1.61
LC019	Armina (RGM – KH)	Silt-mud	58.88	0.88	22.99	9.56	0.05	2.09	0.89	2.29	2.42	0.16	0.03	0.39	1.06
LC020	Armina (RGM – KH)	Silt-mud	62.40	0.86	20.38	8.17	0.06	2.35	0.80	1.86	2.23	0.12	0.02	0.33	1.20
LC021	Armina (RGM – KH)	Grey	65.68	0.97	11.53	9.59	0.28	3.34	5.14	2.32	0.94	0.12	0.04	0.18	0.40
LC022	Armina (RGM – KH)	Grey	67.24	1.11	12.18	10.56	0.17	2.62	3.44	1.70	1.28	0.12	0.07	0.18	0.75
LC023	Armina (RGM – KH)	Grey	64.23	1.12	12.25	10.46	0.22	2.99	4.51	2.11	1.21	0.11	0.05	0.19	0.57
LC024	Armina (RGM – KH)	Grey	65.00	0.97	12.34	9.47	0.24	3.06	4.17	2.99	1.05	0.13	0.04	0.19	0.35
LC027	Armina (RGM – KH)	Silt-mud	63.20	0.76	19.32	8.29	0.06	2.62	0.90	1.51	2.24	0.07	0.04	0.31	1.48
LC028	Armina (RGM – KH)	Silt-mud	61.14	0.74	20.17	8.61	0.06	2.70	0.83	1.66	2.40	0.08	0.03	0.33	1.44
LC029	Armina (RGM – KH)	Silt-mud	64.37	0.91	21.15	7.33	0.01	1.13	0.05	2.00	2.38	0.01	0.02	0.33	1.19
LC030	Armina (RGM – KH)	Silt-mud	60.34	0.87	21.82	9.99	0.15	2.16	0.30	2.20	2.11	0.14	0.03	0.36	0.96
LC031	Armina (RGM – KH)	Silt-mud	61.96	0.77	19.54	10.06	0.16	2.41	0.76	2.31	2.10	0.11	0.03	0.32	0.91
LC032	Armina (RGM – KH)	Grey	67.34	1.00	12.60	9.97	0.13	2.41	2.16	2.06	1.33	0.11	0.05	0.19	0.65
LC033	Armina (RGM – KH)	Grey	65.77	1.06	12.44	10.13	0.19	2.70	3.75	2.22	1.13	0.12	0.08	0.19	0.51
LC034	Armina (RGM – KH)	Grey	72.03	0.69	11.22	6.92	0.23	2.73	3.49	3.03	0.73	0.11	0.04	0.16	0.24
LC036	Armina (RGM – KH)	Grey	63.22	0.81	19.47	8.86	0.13	2.57	0.70	2.59	1.58	0.07	0.03	0.31	0.61
LC041	Armina (RGM – KH)	Grey	66.18	1.01	13.62	8.88	0.30	2.72	2.93	3.16	1.50	0.10	0.04	0.21	0.47
LC044	Armina (RGM – KH)	Grey	69.13	1.00	12.43	9.45	0.14	2.41	3.28	2.10	1.19	0.12	0.04	0.18	0.57
LC046	Armina (RGM – KH)	Grey	61.93	0.86	20.61	10.27	0.12	2.01	0.37	2.27	2.34	0.18	0.03	0.33	1.03
LC047	Armina (RGM – KH)	Grey	61.51	0.84	19.99	10.25	0.10	1.89	0.34	2.45	1.71	0.12	0.03	0.32	0.70
LC048	Armina (RGM – KH)	Grey	59.22	0.83	20.88	11.37	0.07	1.65	0.65	2.75	1.87	0.26	0.03	0.35	0.68
LC049	Armina (RGM – KH)	Grey	59.78	0.81	21.67	9.39	0.10	2.09	0.63	2.87	1.98	0.15	0.02	0.36	0.69
LC050	Armina (RGM – KH)	Grey	57.68	0.87	22.91	10.45	0.07	2.38	0.68	2.55	2.16	0.16	0.03	0.40	0.84
LC051	Armina (RGM – KH)	Silt-mud	58.14	0.89	22.71	10.79	0.09	1.92	0.56	1.77	3.31	0.16	0.02	0.39	1.87
LC052	Armina (RGM – KH)	Silt-mud	57.84	0.90	23.11	10.45	0.04	2.21	0.37	2.53	2.05	0.18	0.03	0.40	0.81
LC053	Armina (RGM – KH)	Silt-mud	56.26	0.90	24.19	10.33	0.09	1.87	0.32	2.55	2.66	0.17	0.02	0.43	1.04
LC054	Armina (RGM – KH)	Grey	56.85	0.90	23.16	9.94	0.07	2.50	0.73	2.77	1.42	0.15	0.03	0.41	0.51
LC055	Armina (RGM – KH)	Grey	59.87	0.83	21.07	9.79	0.09	2.22	1.08	2.30	2.29	0.16	0.03	0.35	1.00
LC056	Armina (RGM – KH)	Silt-mud	65.30	0.73	18.08	8.15	0.12	2.26	1.73	1.62	2.52	0.16	0.03	0.28	1.55
LC060	Armina (RGM – KH)	Silt-mud	62.05	0.88	19.71	8.64	0.10	1.84	1.47	1.61	2.94	0.14	0.03	0.32	1.82
LC061	Armina (RGM – KH)	Grey	62.98	0.81	20.00	8.74	0.10	2.04	1.34	2.01	2.37	0.15	0.02	0.32	1.18
LC062	Armina (RGM – KH)	Silt-mud	59.14	0.71	20.24	7.90	0.06	2.97	1.21	2.06	2.60	0.08	0.02	0.34	1.26
LC063	Armina (RGM – KH)	Silt-mud	61.66	0.80	19.99	9.49	0.07	2.70	0.72	1.85	2.41	0.07	0.03	0.32	1.30

https://doi.org/10.1017/njg.2016.9 Published online by Cambridge University Press

Table 4. Continued.

		wt% →											Al_2O_3/	K_2O/
		Rock type ↓	SiO_2	TiO_2	Al_2O_3	Fe_2O_3	MnO	MgO	CaO	Na_2O	K_2O	P_2O_5	Cr_2O_3	SiO_2	Na_2O
LC064	Armina (RGM – KH)	Grey	60.73	0.80	19.98	9.09	0.11	2.96	0.93	2.30	1.95	0.07	0.05	0.33	0.85
LC065	Armina (RGM – KH)	grey	61.39	0.78	20.95	9.33	0.13	2.41	0.73	3.54	1.71	0.17	0.02	0.34	0.48
LC066	Armina (RGM – KH)	Grey	59.77	0.82	21.66	9.49	0.11	2.32	0.57	2.45	1.61	0.16	0.02	0.36	0.66
LC067	Armina (RGM – KH)	Grey	62.42	0.72	20.88	7.38	0.07	2.45	0.55	2.92	1.52	0.11	0.03	0.33	0.52
LC068	Armina (RGM – KH)	Grey	58.75	0.88	22.08	9.69	0.10	2.18	0.64	3.22	1.72	0.10	0.02	0.38	0.53
LC069	Armina (RGM – KH)	Grey	60.93	0.82	20.65	9.46	0.15	2.27	0.36	2.48	2.50	0.11	0.02	0.34	1.01
LC070	Armina (RGM – KH)	Grey	60.46	0.84	20.17	9.30	0.08	2.16	0.70	2.37	2.51	0.13	0.03	0.33	1.06
LC080	Armina (RGM – KH)	Grey	61.96	0.83	19.14	9.14	0.10	2.58	0.92	2.18	1.94	0.09	0.03	0.31	0.89
LC081	Armina (RGM – KH)	Silt-mud	60.34	0.78	20.78	9.41	0.12	2.31	0.45	3.19	1.89	0.18	0.02	0.34	0.59
LC082	Armina (RGM – KH)	Silt-mud	60.59	0.77	21.83	8.20	0.08	1.98	0.57	2.79	2.55	0.10	0.03	0.36	0.91
LC083	Armina (RGM – KH)	Silt-mud	61.10	0.83	22.08	9.38	0.13	2.41	0.85	2.19	1.84	0.17	0.03	0.36	0.84
LC085	Armina (RGM – KH)	Grey	64.05	0.79	18.91	6.96	0.07	2.46	1.45	2.40	2.03	0.08	0.03	0.30	0.84
LC086	Armina (RGM – KH)	Grey	61.56	0.86	20.54	8.97	0.12	2.61	0.56	2.65	2.10	0.08	0.03	0.33	0.79
LC087	Armina (RGM – KH)	Silt-mud	64.55	0.87	18.75	8.63	0.06	2.52	1.13	2.26	1.92	0.07	0.03	0.29	0.85

RGM, Rosebel Gold Mine; KH, Koolhoven; UCC, Upper Continental Crust; PAAS, Post Archean Australian shales; m-s-g, mudstone-siltstone-greywacke; conglo, conglomerate; grey, greywacke; silt-mud, siltstone-mudstone.

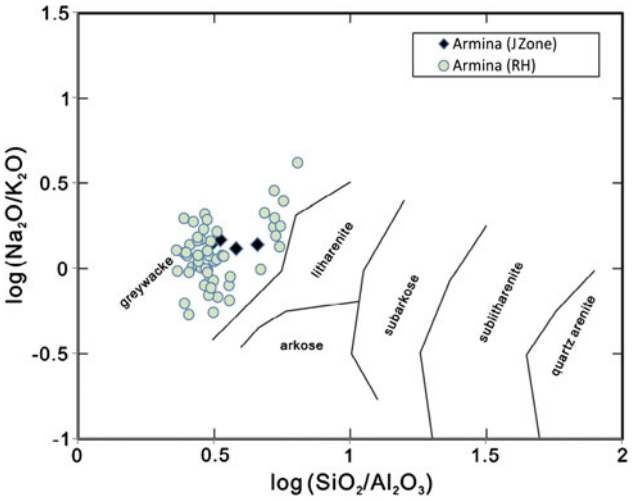

Fig. 23. Classification of the analysed Armina Formation metasedimentary rock samples from RGM according to their logarithmic ratios of SiO_2/Al_2O_3 and Na_2O/K_2O after Pettijohn et al. (1972).

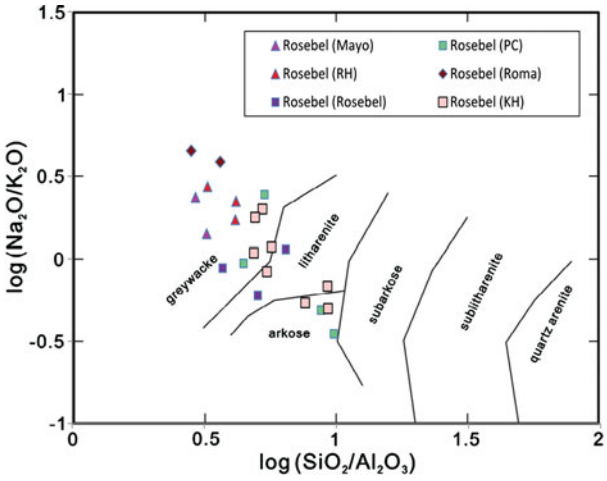

Fig. 24. Classification of the analysed Rosebel Formation metasedimentary rock samples from RGM according to their logarithmic ratios of SiO_2/Al_2O_3 and NaO/K_2O after Pettijohn et al. (1972).

and arkose, those from the Rosebel pit as greywacke and litharenite, the Royal Hill samples as greywacke and the samples of Koolhoven as greywacke, litharenite and arkose. This raises the question of whether not part of those samples should rather have been classified as Armina instead of as Rosebel.

Factor analysis

In order to compare the RGM greywackes with those of the Marowijne, we used the complete dataset including our own samples and the existing data by Daoust et al. (2011) and Carlier (2012) to find distinguishing characteristics between our own four facies, and the Armina and Rosebel Formations within the RGM. Clearly the Pettijohn diagrams based only on few elements are insufficient for that purpose, therefore we applied factor analysis using all elements. From the rotated component matrix (Table 6) three factors are found, which in total explain 66.6% of the variability.

Table 6 shows that Factor 1 is dominated by positive loadings of SiO_2, LMnO and LCaO (the logarithms of MnO and CaO are used because of irregularities in the data), whereas Al_2O_3 and K_2O show high negative loadings. Factor 2 is dominated by

https://doi.org/10.1017/njg.2016.9 Published online by Cambridge University Press

Table 5. Major elements of the samples of the Rosebel Formation from RGM, with the Pay Caro, Mayo, Roma, Rosebel and Royal Hill series samples from Daoust et al. (2011) and the LC series samples from Carlier (2012).

		wt% →												Al_2O_3/	K_2O/
		Rock type ↓	SiO_2	TiO_2	Al_2O_3	Fe_2O_3	MnO	MgO	CaO	Na_2O	K_2O	P_2O_5	Cr_2O_3	SiO_2	Na_2O
		UCC	66.60	0.64	15.40	5.04	0.10	2.48	3.59	3.27	2.80	0.15	0.01	0.23	0.86
Code	**Formation (Location)**	PAAS	62.80	1.00	18.90	7.22	0.11	2.20	1.30	1.20	3.70	0.16	0.02	0.30	3.08
P118934	Rosebel (RGM – PC)	Arenite	70.79	0.70	13.25	7.26	0.07	0.93	2.16	3.15	1.29	0.16	-0.01	0.19	0.41
P118919	Rosebel (RGM – PC)	Arenite	68.15	0.83	15.31	8.32	0.08	1.76	0.66	1.93	2.06	0.11	0.02	0.22	1.06
P118914	Rosebel (RGM – PC)	Arenite	81.10	0.47	9.27	4.58	0.13	0.61	1.56	0.73	1.49	0.02	0.01	0.11	2.04
P118917	Rosebel (RGM – PC)	Arenite	81.08	0.52	8.28	4.85	0.13	0.69	2.09	0.62	1.78	0.05	0.01	0.10	2.85
M118878	Rosebel (RGM – Mayo)	arenite	59.30	0.78	18.35	7.63	0.10	2.04	5.19	3.08	2.17	0.15	0.01	0.31	0.71
M118879	Rosebel (RGM – Mayo)	Conglo	57.57	0.71	19.65	7.32	0.13	1.38	7.46	3.77	1.61	0.14	0.00	0.34	0.43
R118886	Rosebel (RGM – Roma)	Arenite	61.24	0.65	16.85	7.99	0.11	1.96	4.54	4.96	1.28	0.17	0.01	0.28	0.26
R118889	Rosebel (RGM – Roma)	Arenite	56.42	0.58	19.97	6.67	0.10	2.17	5.46	5.10	1.13	0.16	0.00	0.35	0.22
RB118941	Rosebel (RGM – RB)	Arenite	67.84	0.74	18.28	8.03	0.08	1.92	2.18	2.36	2.68	0.14	0.02	0.27	1.14
RB118910	Rosebel (RGM – RB)	Arenite	77.66	0.33	12.06	3.29	0.01	0.51	0.16	2.77	2.43	0.05	0.00	0.16	0.88
RB118912	Rosebel (RGM – RB)	Conglo	66.35	0.90	13.15	9.09	0.13	1.32	3.07	1.99	3.31	0.08	0.02	0.20	1.66
LC006	Rosebel (RGM – KH)	Arenite	76.22	0.31	13.97	2.41	0.04	0.50	1.46	2.63	3.14	0.03	0.04	0.18	1.19
LC007	Rosebel (RGM – KH)	Arenite	75.66	0.18	14.41	1.70	0.03	0.40	1.64	4.37	2.19	0.02	0.05	0.19	0.50
LC008	Rosebel (RGM – KH)	Arenite	76.43	0.26	13.44	2.00	0.03	0.46	1.68	3.22	2.74	0.03	0.04	0.18	0.85
LC009	Rosebel (RGM – KH)	Arenite	73.18	0.21	14.85	1.55	0.03	0.44	1.76	4.53	2.55	0.03	0.03	0.20	0.56
LC017	Rosebel (RGM – KH)	Arenite	69.80	0.73	14.33	6.78	0.10	1.39	2.52	2.27	2.09	0.07	0.04	0.21	0.92
LC057	Rosebel (RGM – KH)	Arenite	77.82	0.52	10.20	4.86	0.11	0.80	1.26	0.94	1.73	0.07	0.04	0.13	1.85
LC058	Rosebel (RGM – KH)	Arenite	79.90	0.61	8.64	6.25	0.12	0.86	1.17	0.86	1.26	0.05	0.09	0.11	1.46
LC059	Rosebel (RGM – KH)	Arenite	81.46	0.48	8.76	4.27	0.11	0.81	1.32	0.78	1.56	0.05	0.04	0.11	2.00
RH118965	Rosebel (RGM – RH)	Arenite	64.50	0.90	15.56	10.94	0.18	2.75	4.09	2.67	1.55	0.12	0.02	0.24	0.58
RH118966	Rosebel (RGM – RH)	Arenite	59.32	0.86	18.22	12.80	0.11	2.24	4.69	4.01	1.47	0.19	0.01	0.31	0.37
RH118953	Rosebel (RGM – RH)	Arenite	64.38	0.84	15.44	9.18	0.07	1.54	3.86	2.09	0.94	0.17	0.01	0.24	0.45

RGM, Rosebel Gold Mine; PC, Pay Caro; RB, Rosebel; KH, Koolhoven; RH, Royal Hill; UCC, Upper Continental Crust; PAAS, Post Archean Australian shales; conglo, conglomerate.

positive loadings of TiO_2, Fe_2O_3 and MgO, and Factor 3 by positive loadings of Na_2O and P_2O_5. The factor scores of all samples from Marowijne and RGM are plotted in Figs 25, 26 and 27.

Fig. 25 (F1–F2) shows the separation along the x-axis (F1) between siliceous (quartz-rich) greywackes on the right side and the aluminum-rich phyllites on the left side. The coincidence of the Marowijne clusters illustrates that the geochemical differences between rocks of different grain size in the same turbidite facies are larger than the differences between the different turbidite facies. The y-axis (F2, representing positive loadings of TiO_2, Fe_2O_3 and MgO) shows samples rich in mafic minerals (i.e. biotite, chlorite, magnetite, ilmenite, garnet) in the upper part of the plot and samples poor in these elements on the lower side. Against expectations, the green metagreywacke and its concretions plot in the Fe_2O_3, MgO, TiO_2-poor and SiO_2-rich regions of the factor analysis. The differences in the results are probably because the selected samples for the analysis are not very rich in chlorite. Only the most mafic-poor samples in the red ellipsoid are considered as belonging to the Rosebel Formation. The others are chemically indistinguishable from Armina Formation rocks.

Table 6. Rotated component matrix.

	Component		
	1	2	3
SiO_2	0.586	−0.527	−0.510
TiO_2	−0.024	0.781	0.082
Al_2O_3	−0.839	0.248	0.354
Fe_2O_3	−0.274	0.799	0.312
MgO	0.085	0.773	−0.155
Na_2O	0.139	0.046	0.771
K_2O	−0.690	0.091	−0.301
P_2O_5	0.044	0.144	0.608
Cr_2O_3	0.403	0.347	−0.611
LMnO	0.723	0.219	−0.072
LCaO	0.809	−0.100	0.128

https://doi.org/10.1017/njg.2016.9 Published online by Cambridge University Press

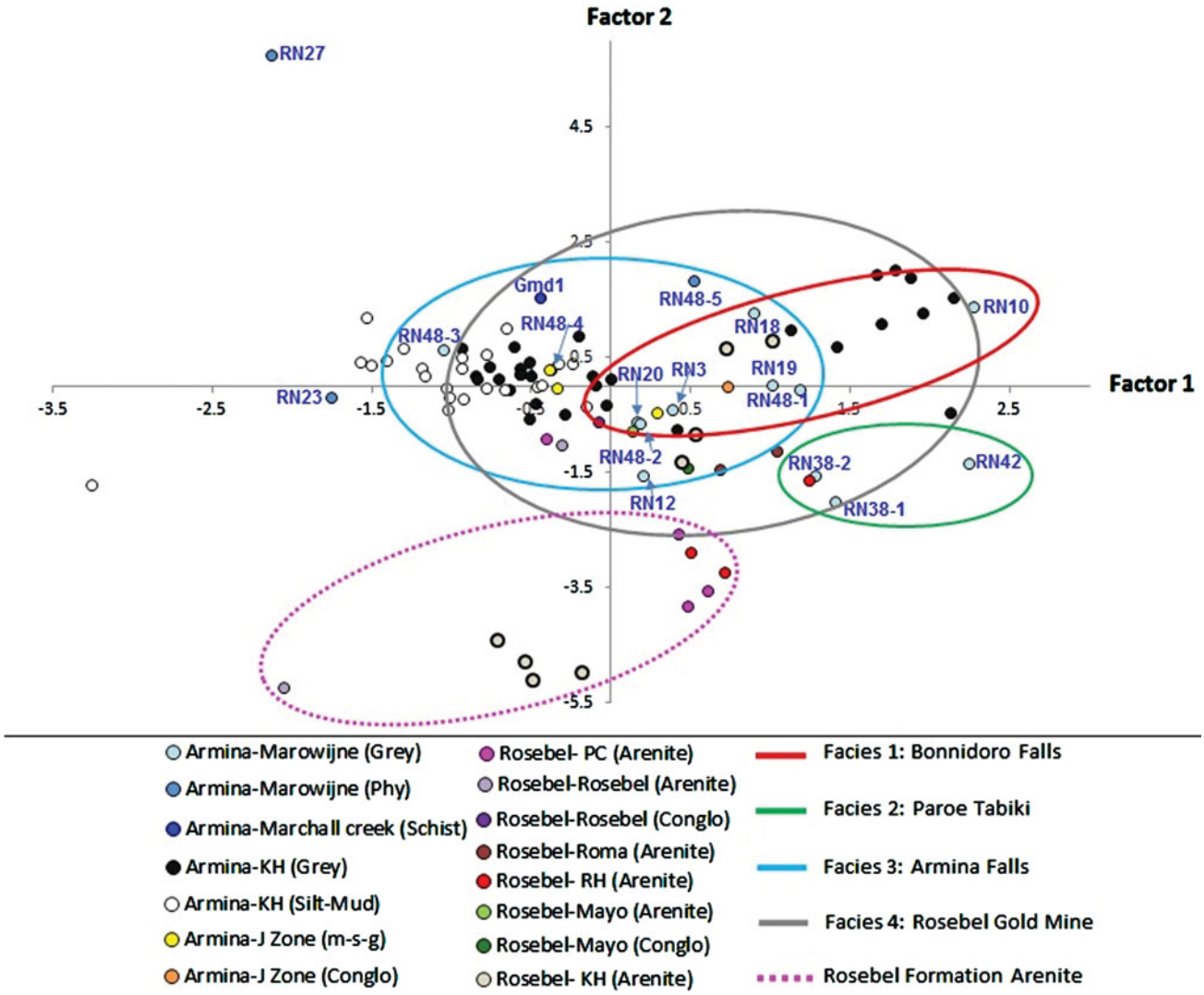

Fig. 25. Factor 1 vs. Factor 2. Factor 1 on the x-axis represents the quartz-rich greywackes on the right side and the aluminum-rich phyllites on the left side, while Factor F2 on the y-axis represents the mafic-rich rocks in the upper part of the plot and the mafic-poor rocks in the lower part.

Fig. 26 (F1–F3) shows the same separation along the x-axis as in Fig. 26, but now the y-axis distinguishes Na-rich (plagioclase) and P-rich (apatite) samples from samples poor in these elements. The role of Cr, a typical element concentrated in mafic igneous rocks, is not clear.

The F2–F3 plot in Fig. 27 is the best plot to show differences between the factor scores of individual samples irrespective of their grain size. It shows a clear separation in Armina Formation samples, which are comparatively rich in plagioclase and mafic minerals, and Rosebel Formation samples (in the red ellipsoid), which are poor in these minerals. This suggests indeed that a large part of the samples which previously was classified as Rosebel Formation by Daoust et al. (2011) and Carlier (2012) in fact may belong to the Armina Formation.

Discussion

Provenance differences between the three facies along the Marowijne River

The point-counting data summarised in Fig. 20 suggest that the three facies exposed along the Marowijne River show subtle differences in composition. From south to north, the greywackes from Bonnidoro Tabiki to Armina Falls increase in quartz content, while the feldspar content decreases. The more resistant quartz is enriched in the northern areas, while the southern areas have more of the less-resistant feldspar. Plutonic fragments decrease also from south to north while monomineralic grains increase in quantity. This may indicate that the differences between the three facies are not caused

https://doi.org/10.1017/njg.2016.9 Published online by Cambridge University Press

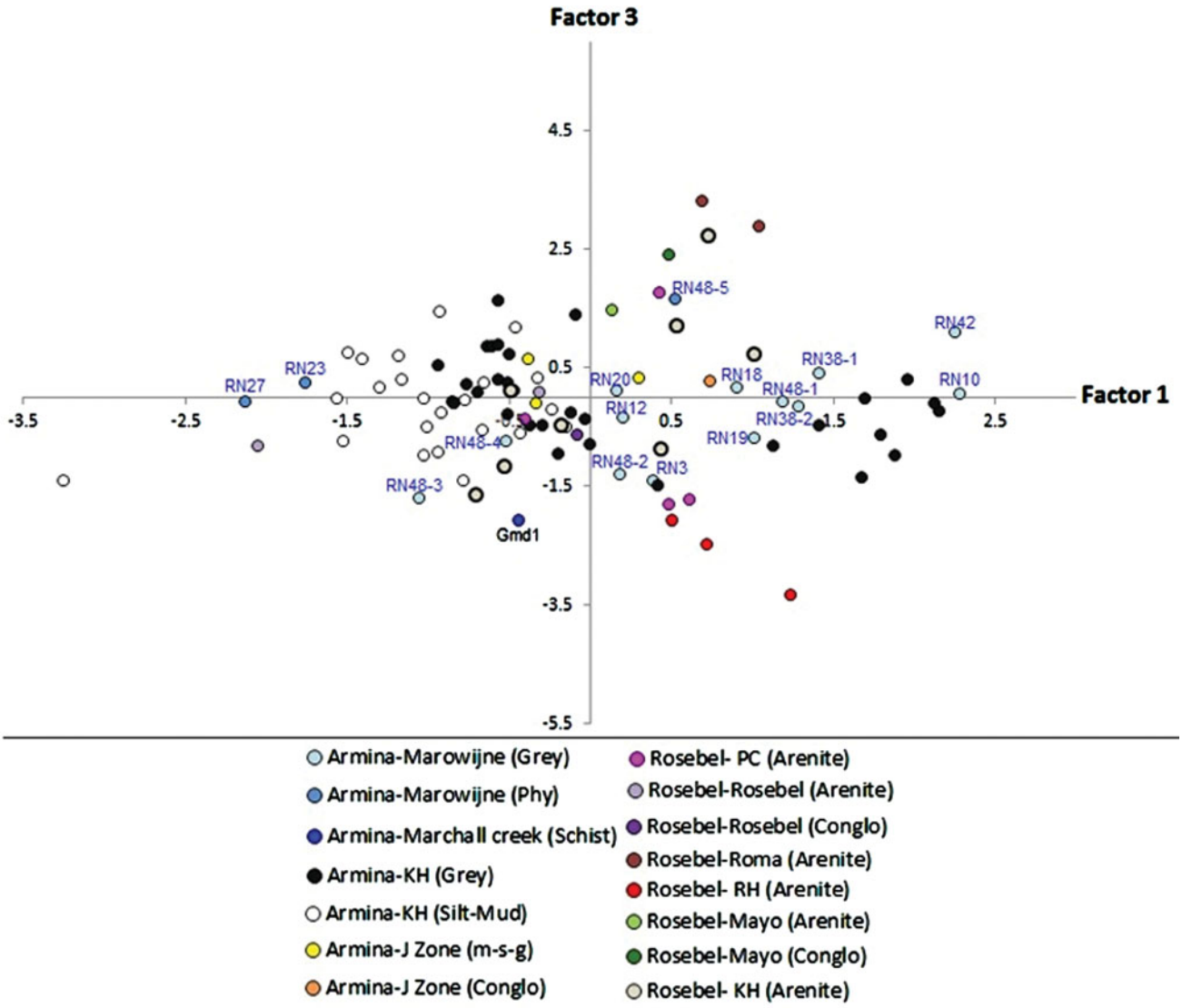

Fig. 26. Factor 1 vs. Factor 3. Factor 3 on the y-axis represents the plagioclase-rich rocks in the upper part of the plot and the plagioclase-poor rocks in the lower part.

by different provenance areas, but probably by differences in weathering and transport of the source rocks. This may imply that the more immature southern Bonnidoro turbidites are older than the northern Armina Falls turbidite. However, the increase in sand-sized quartz content in the metagreywackes of the Armina Falls might also be influenced by the higher grade of metamorphism, as metamorphic recrystallisation increases the size of the crystals.

Provenance differences between metagreywackes from the Marowijne River and RGM

Fig. 20 shows that the metagreywackes from the Marowijne River contain more plutonic fragments than the metagreywackes from RGM, which contain more volcanic fragments. This suggests different source areas. The grain size of the quartz and feldspar clasts in the metagreywackes of the Marowijne River are up to 3 mm; this is a very important indicator for a plutonic instead of a volcanic source area. The plutonic fragments in the metagreywackes of the Marowijne River are probably tonalites (quartz-plagioclase-biotite), which are derived from the TTG plutons. The presence of tonalite fragments in the metagreywackes of the Marowijne River indicates that probably the TTG plutons are older than the metagreywackes. This is supported by age and isotope data from French Guiana (Delor et al., 2003a). The metagreywackes of RGM, on the other hand, contain both mafic and felsic volcanic fragments, which means that these have different source areas.

https://doi.org/10.1017/njg.2016.9 Published online by Cambridge University Press

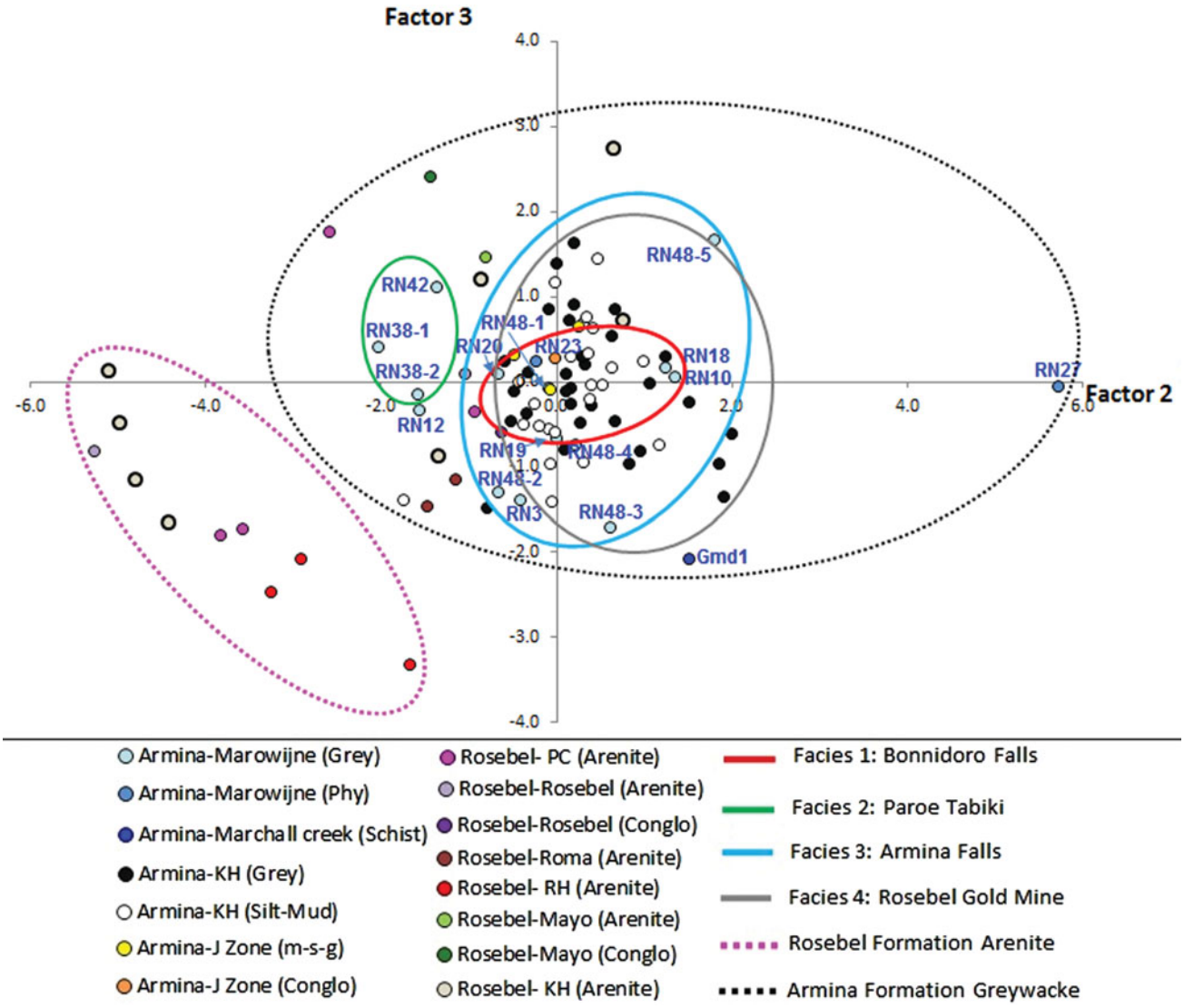

Fig. 27. Factor 2 vs. Factor 3, showing the separation of the Rosebel Formation rocks poor in mafic minerals and plagioclase and the Armina Formation rocks rich in mafic and plagioclase.

Differences between Armina and Rosebel Formations

Factor analysis gives a good distinction between the Armina and Rosebel Formations. The arenite samples from Koolhoven of Carlier (2012), and from Pay Caro and Royal Hill of Daoust et al. (2011) (Fig. 27) seem to be the only 'real' Rosebel Formation arenites. Probably Royal Hill pit is still in the transition zone of Armina and Rosebel because some samples of the Royal Hill pit are plotted as Armina. The other samples from Mayo and Roma of Daoust et al. (2011) are very rich in Fe and poor in Na, which means these 'arenites' are probably greywackes of the Armina Formation. The very mature arenites are poor in Fe_2O_3, MgO and TiO_2, which represent the mafic minerals, and very high in SiO_2. It is suggested that the name Rosebel Formation should only be used for the very mature quartz-rich rocks.

The 'real' quartzarenites and the other immature greywackes of Daoust et al. (2011) (Fig. 27) might be better grouped as Armina Formation. The difference in interpretation might be due to the fact that the contact between these two formations is not clear, and RGM is situated on the contact of the Armina and Rosebel Formations, not in the middle of the syncline basin where probably the very mature arenites predominate. The mature Rosebel arenites have probably been deposited in an epicontinental fluvial environment, from a source area that was much more weathered than any of the source areas of the turbidites.

Conclusions

The Armina Formation metagreywackes show features of deposition by turbidity currents: coarse-grained, poorly sorted

https://doi.org/10.1017/njg.2016.9 Published online by Cambridge University Press

graded greywackes, covered by fine-grained, parallel-laminated phyllites, often with convolute structures and climbing ripples. Their immature composition suggests deposition in an arc-trench environment. The predominance of quartz and plagioclase clasts and tonalite lithic fragments suggests an exhumation of the TTG plutons before deposition of the turbidites. Three facies of metagreywackes can be distinguished along the Marowijne River on the basis of their mineralogy, siderite nodules and calsilicate concretions. Metagreywackes in the southern part of the studied stretch of the Marowijne River might be slightly older than those in the north, on the basis of their more immature character. The metagreywackes of RGM have a predominantly volcanic source area, probably the Paramaka Formation volcanics. This shows that alongstrike the greenstone belt, areas of different surface geology have contributed to the composition of the turbidites, suggesting a more varied paleogeography of the source areas than previously thought. Many rock samples classified in the past as Rosebel Formations might belong on account of their major elements chemistry to the Armina Formation. This requires a reappraisal of the surface geology and sequence of events in the greenstone belt.

Acknowledgements

This research has been supported by a fund from IAMGOLD-Rosebel Gold Mine. We would also like to thank Rosebel Gold Mines for the permission to visit the core-shack and compile the necessary information for this project, with a special note of thanks to Nicole Houle and Caroline Daoust. Louis Carlier is thanked for his willingness to share the data of his research for this project. The Geological and Mining Service of Suriname, especially the head, Mahinder Autar, is thanked for permission to use available data. Professor Theo Wong and Nicole Kioe-A-Sen of the Anton de Kom University are thanked for their support. We would also like to thank the field crew, including Mr Ewald Poetisi of de Anton de Kom University, Benny Pinas and Dwight Lawrence. Otto Stiekema and Leonard Dik of Utrecht University are thanked for preparing the thin sections. Henk Naarendorp and Stephen Essed of FILAB Suriname are thanked for the geochemical analysis. We very much appreciated the willingness of Dr Vriend to help with the factor analysis using SPSS. Kees de Jong and Arike Gill of Naturalis, Leiden, are thanked for their help in tracing the samples collected during early expeditions (1902–1926) along the Marowijne River, and the thin sections prepared from them. Last but not the least the reviewers Professor Poppe de Boer and Dr Dennis LaPoint are thanked for their critical and constructive comments.

References

Blatt, H., ***Middleton, G.*** & ***Murray, R.***, 1980. Origin of Sedimentary Rocks. Prentice-Hall Inc. (New Jersey): 782 pp.

Bosma, W., 1983. Igneous and metamorphic complexes of the Guiana shield in Suriname. Geologie en Mijnbouw 62: 241–254.

Bosma, W. & ***Groeneweg, W.***, 1970. Review of the stratigraphy of Suriname. In: Lee, M. (ed.): Proceedings of the 8th Guiana Geology Conference. Guyana (Georgetown): 1–32.

Bosma, W., ***Kroonenberg, S.***, ***Van Lissa, R.***, ***Maas, K.*** & ***De Roever, E.***, 1977. Geological map of Suriname 1:500,000. Geologisch Mijnbouwkundige Dienst van Suriname.

Bosma, W., ***Kroonenberg, S.***, ***Maas, K.*** & ***de Roever, E.***, 1983. Igneous and metamorphic complexes of the Guiana shield in Suriname. Geologie en Mijnbouw 62: 241–254.

Carlier, L., 2012. Characterization of the geological and geochemical footprint of the Koolhoven gold deposit, Suriname. Thesis, Delft University of Technology (Delft): 151 pp.

Daoust, C., ***Voicu, G.***, ***Brisson, H.*** & ***Gauthier, M.***, 2011. Geological setting of the Paleoproterozoic Rosebel gold district, Guiana Shield, Suriname. Journal of South American Earth Sciences 32: 222–245.

Delor, C., ***Lahondère, D.***, ***Egal, E.***, ***Lafon, J.-M.***, ***Cocherie, A.***, ***Guerrot, C.*** & ***De Avelar, V.***, 2003a. Transamazonian crustal growth and reworking as revealed by the 1:500,000-scale geological map of French Guiana. Géologie de la France 2-3-4: 5–57.

Delor, C., ***de Roever, E.W.***, ***Lafon, J.-M.***, ***Lahondère, D.***, ***Rossi, P.***, ***Cocherie, A.*** & ***Potrel, A.***, 2003b. The Bakhuis ultra-high-temperature granulite belt (Suriname): II. Implications for the late Transamazonian crustal stretching in a revised Guiana Shield framework. Géologie de la France 2-3-4: 207–230

De Munck, V., 1954a. Blad Java, C8. Geologisch Mijnbouwkundige Dienst van Suriname. N.V. drukkerij 'Eldorado' (Paramaribo): 20 pp.

De Munck, V., 1954b. Blad Bigiston, C9. Geologisch Mijnbouwkundige Dienst van Suriname. N.V. drukkerij 'Eldorado' (Paramaribo): 19 pp.

De Munck, V., 1954c. Blad Nassau, D8. Geologisch Mijnbouwkundige Dienst van Suriname. N.V. drukkerij 'Eldorado' (Paramaribo): 108 pp.

De Vletter, D.R., 1984. Synthesis of the Precambrian of Suriname and review of some outstanding problems. Geologisch Mijnbouwkundige Dienst van Suriname, Mededelingen 27: 11–31.

Dickinson, W., 1970. Interpreting detrital modes of graywacke and arkose. Journal Sedimentology Petrology 40: 695–707.

Dickinson, W.R., ***Beard, L.S.***, ***Brackenridge, G.R.***, ***Erjavec, J.L.***, ***Ferguson, R.C.***, ***Inman, K.F.***, ***Knepp, R.A.***, ***Lindberg, F.A.*** & ***Ryberg, P.T.***, 1983. Provenance of North American Phanerozoic sandstones in relation to tectonic setting. Geological Society of America Bulletin 94: 222–235.

Folk, R. L., 1951. Stages of textural maturity in sedimentary rocks. Journal of Sedimentary Petrology 21: 128.

Gibbs, A. & ***Barron, C.***, 1993. The Geology of the Guyana Shield. In: Monographs on Geology and Geophysics 22. Oxford University Press (New York): 246 pp.

Herron, M. M., 1988. Geochemical classification of terrigenous sands and shales for core or log data. Journal of Sedimentary Petrology 58: 820–829.

Hunter, R., 1977. Terminology of cross-stratified sedimentary layers and climbing-ripple structures. Journal of Sedimentary Petrology 47: 697–706.

Hurley, P.M., ***De Almeida, F.F.M.***, ***Melcher, G.C.***, ***Cordani, U. G.***, ***Rand, J.R.***, ***Kawashita, K.***, ***Vandoros, P.***, ***Pinson, W.H.*** & ***Fairbairn, H.W.*** 1967. Test of continental drift by comparison of radiometric ages. Science 157: 495–500.

https://doi.org/10.1017/njg.2016.9 Published online by Cambridge University Press

Ingersoll, R.V., ***Bullard, T.F.***, ***Ford, R.L.***, ***Grimm, J.P.***, ***Pickle, J.D.*** & ***Sares, S.W.***, 1984. The effect of grain size on detrital modes: A test of the Gazzi–Dickinson point-counting method. Journal of Sedimentary Petrology 54: 103–116.

Kroonenberg, S.B. & ***De Roever, E.W.***, 2010. Geological evolution of the Amazonian Craton. In: Hoorn, C. and Wesselingh, F.P. (eds): Amazonia, Landscape and Species Evolution. Blackwell Publishing: 7–28.

Kroonenberg, S.B., ***De Roever, E.W.F.***, ***Fraga, L.M.***, ***Reis, N.J.***, ***Faraco, M.T.***, ***Cordani, U.G.***, ***Lafon, J.-M.*** & ***Wong, Th.E.***, 2016. Paleoproterozoic evolution of the Guiana Shield in Suriname – a revised model. Netherlands Journal of Geosciences (this volume) 10.1017/njg.2016.10.

Marot, A. & ***Capdevila, R.***, 1980. Géologie du Synclinorium du Sud de Guyana Francaise. Conferencia Geologica del Caribe (Santo Domingo): 613–618.

Pettijohn, F., ***Potter, P.E.*** & ***Siever, R.***, 1972. Sand and Sandstone. Springer-Verlag (New York): 618 pp.

Rudnick, R. & ***Gao, S.***, 2003. Composition of the continental crust. The Crust 3: 1–64.

Taylor, S. & ***McLennan, S.***, 1985. The Continental Crust: its Composition and Evolution. Blackwell Scientific Publication (Palo Alto): 312 pp.

Vanderhaeghe, O., ***Ledru, P.***, ***Thiéblemont, D.***, ***Egal, E.***, ***Cocherie, A.***, ***Tegyey, M.*** & ***Milési, J.P.***, 1998. Contrasting mechanism of crustal growth: Geodynamic evolution of the Paleoproterozoic granite–greenstone belts of French Guiana. Precambrian Research 92: 165–193.

IJzerman, R., 1931. Outline of the geology and petrology of Surinam (Dutch Guiana). Kemink & Zoon N.V. (Utrecht): 519 pp.

https://doi.org/10.1017/njg.2016.9 Published online by Cambridge University Press